

## Accepted Manuscript

The Interplay between Molecular Layering and Clustering in Adsorption of Gases on Graphitized Thermal Carbon Black - Spill-Over Phenomenon and the Important Role of Strong Sites

D.D. Do, S.L. Johnathan Tan, Yonghong Zeng, Chunyan Fan, Van T. Nguyen, Toshihide Horikawa, D. Nicholson

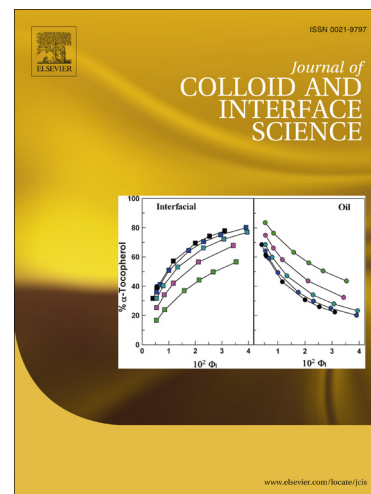
PII: S0021-9797(15)00063-6  
DOI: <http://dx.doi.org/10.1016/j.jcis.2015.01.028>  
Reference: YJCIS 20170

To appear in: *Journal of Colloid and Interface Science*

Received Date: 5 December 2014  
Accepted Date: 13 January 2015

Please cite this article as: D.D. Do, S.L. Johnathan Tan, Y. Zeng, C. Fan, V.T. Nguyen, T. Horikawa, D. Nicholson, The Interplay between Molecular Layering and Clustering in Adsorption of Gases on Graphitized Thermal Carbon Black - Spill-Over Phenomenon and the Important Role of Strong Sites, *Journal of Colloid and Interface Science* (2015), doi: <http://dx.doi.org/10.1016/j.jcis.2015.01.028>

This is a PDF file of an unedited manuscript that has been accepted for publication. As a service to our customers we are providing this early version of the manuscript. The manuscript will undergo copyediting, typesetting, and review of the resulting proof before it is published in its final form. Please note that during the production process errors may be discovered which could affect the content, and all legal disclaimers that apply to the journal pertain.



# The Interplay between Molecular Layering and Clustering in Adsorption of Gases on Graphitized Thermal Carbon Black - Spill-Over Phenomenon and the Important Role of Strong Sites

D. D. Do<sup>a,\*</sup>, S.L. Johnathan Tan<sup>a</sup>, Yonghong Zeng<sup>a</sup>, Chunyan Fan<sup>b</sup>, Van T. Nguyen<sup>a</sup>, Toshihide Horikawa<sup>c</sup>, D. Nicholson<sup>a</sup>

<sup>a</sup>School of Chemical Engineering, University of Queensland, St. Lucia, Qld 4072, Australia

<sup>b</sup>Department of Chemical Engineering, Curtin University, Bentley, WA 6102, Australia

<sup>c</sup>Department of Advanced Materials, Institute of Technology and Science, University of Tokushima, 2-1 Minamijosanjima, Tokushima 770-8506, Japan

\*Corresponding author.

## Abstract

We analyse in detail our experimental data, our simulation results and data from the literature, for the adsorption of argon, nitrogen, carbon dioxide, methanol, ammonia and water on graphitized carbon black (GTCB), and show that there are two mechanisms of adsorption at play, and that their interplay governs how different gases adsorb on the surface by either: (1) molecular layering on the basal plane or (2) clustering around very strong sites on the adsorbate whose affinity is much greater than that of the basal plane or the functional groups. Depending on the concentration of the very strong sites or the functional groups, the temperature and the relative strength of the three interactions, (a) fluid-strong sites (fine crevices and functional group) (F-SS), (b) fluid-basal plane (FB) and (c) fluid-fluid (FF), the uptake of adsorbate tends to be dominated by one mechanism. However, there are conditions (temperature and adsorbate) where two mechanisms can both govern the uptake. For simple gases, like argon, nitrogen and carbon dioxide, adsorption proceeds by molecular layering on the basal plane of graphene, but for water which represents an extreme case of a polar molecule, clustering around the strong sites or the functional groups at the edges of the graphene layers is the major mechanism of adsorption and there is little or no adsorption on the basal planes because the F-SS and FF interactions are far stronger than the FB interaction. For adsorptives with lower polarity, exemplified by methanol or ammonia, the adsorption mechanism switches from clustering to layering in the order: ammonia, methanol; and we suggest that the bridging between these two mechanisms is a molecular spill-over phenomenon, which has not been previously proposed in the literature in the context of physical adsorption.

## 1. Introduction

Adsorption of gases on carbon black at sub-critical temperatures, has been generally regarded as being a molecular layering process. Graphitized thermal carbon black (GTCB) is considered to be an especially appropriate adsorbent in this respect because of the energetic homogeneity of the graphite basal plane. Irving Langmuir in 1917 was the first to describe the sub-monolayer adsorption process, and the theory was later extended by Brunauer, Emmett and Teller in 1938 to multilayer adsorption, widely known as the *BET* theory. In Langmuir's theory, interactions among adsorbate molecules are ignored, and in the *BET* theory it is assumed that these interactions are equivalent to those in the liquid state in the adsorbate beyond the first adsorbed layer. Since the pioneering work of Langmuir and

Brunauer and co-workers, many modifications to the multilayer theory have been proposed (Do, 1998). Cassel (1944) was perhaps the first to highlight one of the limitations of the *BET* theory by pointing out that if the lateral interactions are ignored the surface tension becomes negative and even infinitely negative. With the introduction of molecular simulation the potential energy of interaction between adsorbate molecules, and between adsorbate molecules and the adsorbent surface can be specifically accounted for. The mechanism of adsorption can now be probed in microscopic detail and many simulation results have been achieved which are in agreement with the experimental data.

*GTCB* particles have a polyhedron shape (Schaeffer *et al.*, 1953; Graham and Kay, 1961; Yoshizawa *et al.*, 2006, 2008, 2010), and despite its homogeneous basal plane it possesses high energy sites at the junctions between the adjacent basal planes (Donnet, 1993, 1994). These sites could be due to functional groups which are not removed in the process of graphitization but very fine crevices (defects) at these junctions may also make a contribution. The importance of functional groups has been highlighted in many papers, for example: Bandosz *et al.* (1996), Taqvi and LeVan (1997), Salame and Bandosz (1999, 2002), Toth and Laszlo (2012) and Seredych *et al.* (2014). Irrespective of their origin, these strong sites can act as locations for anchoring adsorbate molecules. If the strong sites are due to functional groups, which always carry fixed partial charges, interaction with associating fluids, such as water and ammonia, will be primarily associated with electrostatic interactions. The combination of the defects and the functional groups will enhance the initial interaction of associating fluids with the carbon surface, no matter how low their adsorption capacity. This results in the formation of a physically bound complex, which then acts as a nucleating site for further adsorbate molecules to adsorb and grow into a cluster. This is the clustering mechanism, that has been reported in the literature (for example, Cassell, 1944). In the case of highly graphitised carbons, explanations of the observed isotherms based on a high concentration of narrow pores can clearly be ruled out, nevertheless these adsorbents exhibit strong water uptake (Belyakova *et al.*, 1968) in the form of type III isotherms. Graphitisation at extremely high temperature (approaching 3000K) destroys or removes most functional groups as well as increasing particle size and reducing surface area per unit mass. However, the very large number of edge sites per particle is likely to ensure that residual electrostatic charge and breaks in the basal planes will be present at the edges. Although there are reports stating that highly graphitized carbon blacks have no

oxygen-containing groups on the surface, because they are decomposed at high temperatures, evidence suggests that a small quantity of these groups remains even after graphitization at high temperature (Campanella *et al.*, 1982; Bruner *et al.*, 1976; Zettlemyer, 1968; Healy *et al.*, 1955; Smith *et al.*, 1956; Young *et al.*, 1954).

Thus it is clear that there are two distinct groups of sites for adsorption on the surface of *GTCB*: (1) the basal plane and (2) the defects and the functional groups. In this paper, we analyse the extensive experimental data for a number of adsorptives to show the interplay between molecular layering and clustering (that are commonly known in the literature), and an intermediate state between these two extremes which we introduce as a previously unrecognised phenomenon: spill-over in physical adsorption. We discuss argon, nitrogen, carbon dioxide, methanol, ammonia and water as adsorptives to cover a range of different hydrogen bond strengths in the order: argon, nitrogen  $\ll$  carbon dioxide  $\ll$  methanol  $<$  ammonia  $<$  water.

Argon and nitrogen are chosen to demonstrate the dominance of the fluid-basal plane interaction as one extreme, and water to show the dominance of the functional group at the other. The adsorptives with intermediate electrostatic strength (methanol and ammonia) exemplify the spill-over phenomenon.

We shall use two theoretical tools to study the behaviour of adsorption for these gases. The first is the Henry law constant, which is a measure of the strength of the affinity between an adsorbate molecule and the strongest sites on the surface. This helps to distinguish between the molecule-basal plane interaction and the interaction of a molecule with strong sites. For solids in general, the energy of adsorption sites can be widely distributed, and complications can arise because of uncertainties about the spatial arrangement of these sites. This is outside the scope of this paper. The second tool we use to analyse adsorption on *GTCB* is Monte Carlo simulation over the region of monolayer coverage and beyond. This gives a direct insight into the way in which the cohesive forces between adsorbate molecules order molecular clustering.

Gases adsorbed on the very homogeneous basal plane of *GTCB* are expected to be mobile, while adsorption on defects and/or functional groups is localised. Those gases that do not interact specifically with strong sites will adsorb on the basal plane according to a molecular layering mechanism and, at zero loading, we can quantify them with the theoretical Henry

constant and isosteric heat Do *et al.* (2008). On the other hand, for adsorptives that form associating fluids, adsorption on functional groups dominates the value of the Henry constant. Once a gas-functional group complex has been formed it acts as an anchor for further adsorption through co-operative hydrogen bonding.

Chemical heterogeneities (Jorge *et al.*, 2002), often as functional groups attached to the graphene surface, (Birkett and Do, 2007; McCallum *et al.*, 1998; Liu and Monson, 2006; Lodewyckx and Vansant, 1999, Muller *et al.*, 1996) have been invoked as an explanation for the experimental observations of water (and other associating fluids) adsorption on carbon material. However, theoretical considerations suggest that attachment to the surface of the basal plane is improbable, and that the dangling bonds at edge sites, leading to localised charge density are a more probable location for functional groups (Morimoto and Miura, 1985-1991), or indeed it is possible that the edge charges alone are sufficient to nucleate water adsorption (Nakada *et al.*, 1996; Segara and Glandt, 1994; Ohba and Kanoh, 2012).

## 2. Theory

The development of a theory for the Henry constant was described in detail in Do *et al.* (2008) and here we briefly present its features for a solid composed of a basal plane and functional groups (together with defects at the edges to form strong sites) attached to the edges of the graphene layers.

### 2.1 Adsorbate potential

Argon is modelled as a simple Lennard-Jones (LJ) molecule. Its collision diameter and reduced well depth are 0.3405nm and 119.8K, respectively. The intermolecular potential energy of interaction of the weakly polar nitrogen is described by the TraPPE model, which has two LJ sites and three electrostatic sites (Potoff and Siepmann, 2001): the collision diameter and reduced well depth for the nitrogen model are 0.331nm and 36K, respectively. One positive charge (0.964e) was placed at the centre of the molecular axis joining the centres of nitrogen atoms and two symmetric negative charges (-0.482e) on two nitrogen atoms at a bond length of 0.11nm. For carbon dioxide, we used the TraPPE model (Potoff and Siepmann, 2001), which has three LJ sites and three fixed partial charges. The C=O bond length is 0.116nm, and the collision diameter, the reduced well depth of interaction energy for C- and O-LJ sites and the partial charges are listed in Appendix 1. For methanol

we also used the TraPPE potential model (Chen *et al.*, 2001). This model has two LJ sites (on the methyl group and on the oxygen atom), and three fixed partial charges on the methyl group, on the oxygen atom and on the hydrogen atom. For ammonia we used the model proposed by Kristof *et al.* (1999) with one LJ site and four fixed partial charges. The rigid non-polarizable polyatomic SPC/E model of Berendsen *et al.* (1987) was used to model water. This model has a single LJ site located at the centre of the oxygen atom and three fixed point charges representing the charge distribution of the molecule. Two positive charges ( $q^+$ ) are located at the centres of the hydrogen atoms, and a single negative charge ( $q^-$ ) is located at the centre of oxygen atom. The molecular parameters for methanol, ammonia and water models are listed in Appendix 1.

## 2.2 Henry constant

The amount of pure component adsorbed on a solid adsorbent at very low loadings can be expressed by the following Henry's law:

$$C = K(P / R_g T) \quad (1)$$

where  $C$  is the surface excess concentration,  $P$  is the absolute pressure,  $R_g$  is the gas constant,  $T$  is the temperature of the system and  $K$  is the Henry constant. The Henry constant  $K$ , is a measure of the interaction between a single molecule and the solid which includes all adsorption sites on the adsorbent and, as mentioned in the Introduction, the strongest sites will dominate the Henry constant. In the specific example of a graphene surface with functional groups (and/or defects) grafted at the edges we are interested in the contribution that these groups will make to Henry law adsorption. To distinguish these, we will determine the Henry constant for the basal plane and that for the functional group separately.

For a given volume of solid,  $\Omega$  in a simulation box containing solid atoms and void space, whose volume is  $V_\Omega$  divided by an interface where adsorption is taking place, let the interaction energy between an adsorbate molecule at any point  $\underline{r}$  and all solid atoms be  $\phi(\underline{r})$ . The local density at any point  $\underline{r}$  is related to the bulk gas density,  $\rho_b$ , according to the Boltzmann distribution law

$$\rho(\underline{r}) = \rho_b \exp[-\phi(\underline{r}) / kT] \quad (2)$$

The number of molecules that can be found in a differential volume  $d\underline{r}$  is  $\rho(\underline{r})d\underline{r}$ . Therefore the total number of particles in the simulation box when there is no interaction between adsorbate molecules (i.e. dilute conditions) is

$$N = \rho_b \int_{\Omega} \exp[-\varphi(\underline{r})/kT] d\underline{r} \quad (3)$$

In experiments, the concentration of the adsorbed phase is determined as an excess amount defined as the difference between the total amount in the volume  $\Omega$  (eq.3) and the amount that would occupy an apparent volume  $V_{app}$  (see below) at the density of the bulk phase is

$$N^{ex} = \rho_b \int_{\Omega} \exp[-\varphi(\underline{r})/kT] d\underline{r} - V_{app} \rho_b \quad (4)$$

We can define the intrinsic Henry constant as the ratio of the excess amount to the bulk gas density.

$$K_{intrinsic} \stackrel{DEF}{=} \left( \frac{N^{ex}}{\rho_b} \right) = \int_{\Omega} \exp[-\varphi(\underline{r})/kT] d\underline{r} - V_{app} \quad (5)$$

This constant has units of volume (expressed here in  $\text{nm}^3$ ), and its physical meaning is the volume that would be occupied by the adsorbate if this excess amount is allowed to expand to the bulk gas density.

Given the excess quantity, the surface excess density of the adsorbed phase is defined as the ratio of the excess quantity to the interfacial surface area of the solid:

$$\Gamma = \frac{N^{ex}}{A} = \frac{1}{A} \left\{ \int_{\Omega} \exp\left[-\frac{\varphi(\underline{r})}{kT}\right] d\underline{r} - V_{app} \right\} \rho_b \quad (6a)$$

The surface Henry constant is then defined as the ratio of the excess density to the bulk gas density:

$$K_A = \frac{1}{A} \left\{ \int_{\Omega} \exp\left[-\frac{\varphi(\underline{r})}{kT}\right] d\underline{r} - V_{app} \right\} = \frac{K_{intrinsic}}{A} \quad (6b)$$

The Henry constant with respect to an interfacial area has units of length (expressed in nm).

Similarly, the volumetric excess density in a confined space of a pore is defined as the ratio of the excess quantity to the pore volume of the solid:

$$\rho_A = \frac{N^{ex}}{V} = \frac{1}{V} \left\{ \int_{\Omega} \exp \left[ -\frac{\varphi(\underline{r})}{kT} \right] d\underline{r} - V_{app} \right\} \rho_b \quad (7a)$$

from which the volumetric Henry constant (which is dimensionless) is:

$$K_V = \frac{1}{V} \left\{ \int_{\Omega} \exp \left[ -\frac{\varphi(\underline{r})}{kT} \right] d\underline{r} - V_{app} \right\} = \frac{K_{intrinsic}}{V} \quad (7b)$$

There are many different ways to define the apparent volume and this has been the subject of considerable debate in the literature. It is clear from eq. (4) that the amount adsorbed is a calculated quantity and the choice of  $V_{app}$  is a difficulty facing experimentalists. Here we consider four possible choices:

1. The same as the volume of the system, which includes the solid volume, i.e.  $V_{\Omega}$
2. The helium void volume,  $V_{He}$
3. The absolute volume, which extends to the surface passing through the centres of the atoms at the outermost surface of the solid,  $V_{abs}$
4. The accessible volume,  $V_{acc}$

#### System volume, $V_{\Omega}$

We consider the two systems as shown in Figure 1. Both systems have exactly the same void volume and the same interface. The only difference between them is that system 2 has a larger adsorbent volume; i.e. a larger  $\Omega$ . If these systems are exposed to the same pressure, the adsorption is the same in both because they have the same interfacial area. This means that the numbers of molecules in the two systems are the same ( $N$  in eq.3), but the excess amount, as defined in eq. (4), will be less in system 2 because of its larger volume, and can even be negative if the volume  $V_{\Omega}$  is very large. This problem arises in the net adsorption defined by Gumma and Talu (2010). Clearly this net adsorption does not reflect the state of the adsorbed phase as it does not give a measure of how dense the adsorbed phase is.



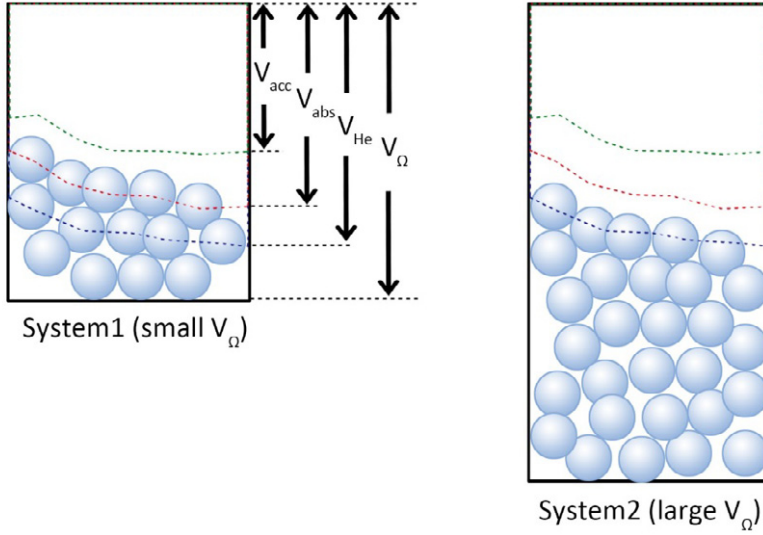


**Figure 1:** Schematics of two systems having the same gas volume and the same interface between the gas and solid phases. System 2 has a larger solid volume.  $V_{\Omega}$  is the volume of the whole system.  $V_{He}$  is the blue dashed line,  $V_{abs}$  is the red dashed line and  $V_{acc}$  is the green dashed line.

#### Helium void volume, $V_{He}$

In experimental procedures, helium is commonly used to obtain the “apparent” void volume (it must be emphasised that this is apparent and not geometrical). Experimentally, this is measured by dosing a known amount of helium into the system at a temperature  $T_{He}$  (which may be different from the adsorption temperature  $T$ ) where the He concentration is quite low. Eq.(3) is also valid for helium, and therefore:

$$N_{He} = \rho_{He} \int_{\Omega} \exp[-\phi_{He}(\underline{r}) / kT_{He}] d\underline{r} \quad (8)$$

where  $\rho_{He}$  is the density of helium in the bulk phase and  $\phi_e$  is the helium-solid potential energy. The helium void volume,  $V_{He}$ , is defined as the one that gives zero excess amount:

$$V_{He} = N_{He} / \rho_{He} = \int_{\Omega} \exp[-\phi_{He}(\underline{r}) / kT_{He}] d\underline{r} \quad (9)$$

Since some helium adsorbs at  $T_{He}$  (even though  $\phi_{He}$  may be very weak)  $V_{He}$  is always greater than the actual void volume of the system and is a function of temperature. The problem of helium adsorption was encountered by Malbrunot and co-workers in 1992, and rectified by high temperature helium expansion in 1997.

Absolute void volume,  $V_{abs}$ 

If helium expansion is carried out at higher temperatures and extrapolated to the limit of infinite temperature the helium volume then becomes an absolute void volume which is independent of the probe gas and temperature (Steele and Halsey, 1955). This absolute void volume is the volume of free space extending right up the boundary that passes through the centres of solid atoms residing in the outermost layer (the red dashed line in Figure 1), i.e.

$$V_{abs} = \lim_{T \rightarrow \infty} V_{app}(\alpha, T) < V_{app}(\alpha, T) \quad (10)$$

where  $\alpha$  represents the probe gas. For this absolute volume, the surface Henry constant is:

$$K_A = \frac{1}{A} \left\{ \int_{\Omega} \exp \left[ -\frac{\phi(\underline{r})}{kT} \right] d\underline{r} - V_{abs} \right\} \quad (11)$$

Since the solid-fluid potential energy is either infinite or a very large positive number in the solid region of the volume  $\Omega$  the integral in the first term on the *RHS* of eq. (11) is essentially zero inside the volume ( $V_{\Omega} - V_{abs}$ ). Therefore, the range of the integration is effectively limited to the absolute volume (red dashed line in Figure 1):

$$K_A = \frac{1}{A} \left\{ \int_{V_{abs}} \exp[-\phi(\underline{r})/kT] d\underline{r} - V_{abs} \right\} = \frac{1}{A} \int_{V_{abs}} \{ \exp[-\phi(\underline{r})/kT] - 1 \} d\underline{r} \quad (12)$$

This equation is used regularly in the literature. For a system in which the potential is varying in only one dimension, we can write:

$$K = \int_0^{\infty} \{ \exp[-\phi(z)/kT] - 1 \} dz \quad (13)$$

The origin is at the surface passing through centres of atoms in the outermost layer of the adsorbent. Figure 2 shows schematically the difference between the two terms in the integrand on the *RHS* of eq.(13). The first integral is the area under the curve of the Boltzmann factor and the second integral is the area under the horizontal dashed line. When the area of the region I is less than that of region II, which will happen at sufficiently high temperatures, the Henry constant becomes negative (Do *et al.*, 2008), which is not physically acceptable.

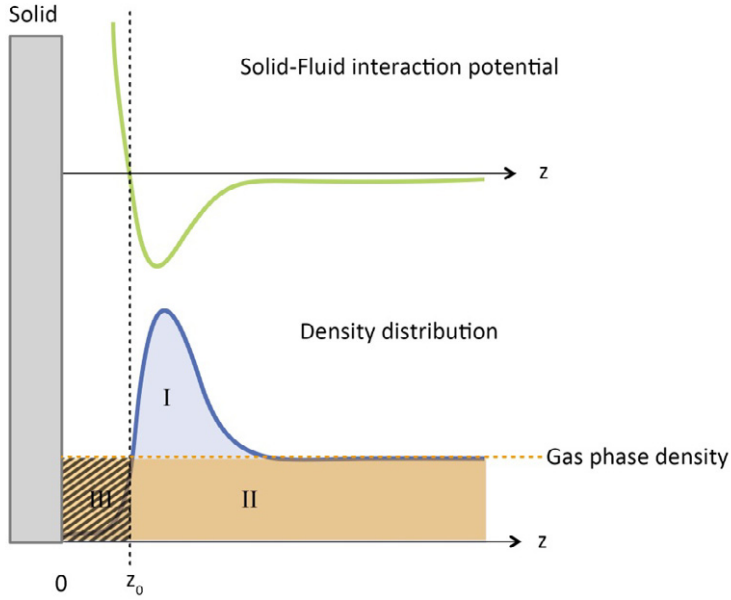


**Figure 2:** Local density distribution versus distance from a solid surface

#### Accessible void volume, $V_{acc}$

One way to avoid the negative Henry constants that could occur in the above choices of void volume is to use the accessible volume suggested by Do and Do (2006) which is specific to the adsorbate under consideration. This is the volume in which the solid-fluid potential energy is non-positive. In this case we write the surface Henry constant as:

$$K_A = \frac{1}{A} \int_{\Omega} \left\{ \exp[-\phi(r)/kT] - H[-\phi(r)] \right\} dr \quad (14a)$$

where  $H$  is the Heaviside step function. For one-dimensional systems, this equation is:

$$K_A = \int_0^{\infty} \left\{ \exp[-\phi(z)/kT] - H(z - z_0) \right\} dz \quad (14b)$$

Here  $z_0$  is the position at which the potential between an adsorbate molecule and the adsorbent is zero. This definition of the surface Henry constant ensures that its value is always positive. Eq. (14b) will be used in this paper to compute the surface Henry constant for argon on the basal plane of the graphene layers. For other adsorbates (nitrogen, carbon dioxide, methanol, ammonia and water) where the potential varies with orientation, the appropriate equation is:

$$K_A = \int_{\omega_0}^{\infty} \left\{ \exp[-\phi(z, \omega) / kT] - H(z - z_0) \right\} dz d\omega \quad (14c)$$

The potential is calculated from the Steele 10-4-3 equation. The graphene surface has a surface density of  $38.2 \text{ nm}^{-2}$ , with a separation distance of  $0.335 \text{ nm}$  between graphene layers. The LJ parameters for a carbon atom in a graphene layer are  $\sigma_s = 0.34 \text{ nm}$  and  $\epsilon_s/k_B = 28 \text{ K}$  (Crowell, 1958).

#### Henry constant with respect to a functional group:

The Henry constant between a molecule and functional group  $\alpha$   $K_\alpha$  can be calculated by integrating the Boltzmann factor over the volume space around the functional group and over all possible orientations of the molecule (Do *et al.*, 2008):

$$K_\alpha = \iint_{\Omega, \omega} \left\{ \exp[-\phi(\mathbf{r}, \omega) / kT] - H[-\phi(\mathbf{r}, \omega)] \right\} d\mathbf{r} d\omega \quad (15)$$

where  $\phi$  is the potential energy of interaction between an adsorbate molecule at the position  $\mathbf{r}$  and orientation  $\omega$  with a functional group grafted at the edge of the graphene layers.  $K_\alpha$  has the dimensions of a volume ( $\text{nm}^3$ ), and is the intrinsic Henry constant defined earlier in Eq.(5). Details of the adsorbent are given in Section 2.4. The intermolecular interaction energy between a fluid molecule  $i$  and a functional group  $j$ ,  $\phi_{i,j}$ , is given by the summation of the 12-6 LJ interaction and the Coulombic interaction:

$$\phi_{i,j} = 4 \sum_{\alpha=1}^A \sum_{\beta=1}^B \epsilon_{i,j}^{\alpha,\beta} \left[ \left( \frac{\sigma_{i,j}^{\alpha,\beta}}{r_{i,j}^{\alpha,\beta}} \right)^{12} - \left( \frac{\sigma_{i,j}^{\alpha,\beta}}{r_{i,j}^{\alpha,\beta}} \right)^6 \right] + \frac{1}{4\pi\epsilon_0} \sum_{c=1}^C \sum_{d=1}^D \frac{q_i^c q_j^d}{r_{i,j}^{c,d}} \quad (16)$$

where parameter  $\epsilon_{i,j}^{\alpha,\beta}$  is associated with a site  $\alpha$  on  $i$  and a site  $\beta$  on  $j$ . The parameters  $\sigma$  and  $\epsilon$  are the collision diameter and the well depth of interaction energy, respectively. The three functional groups considered in this work are carbonyl, hydroxyl and carboxyl groups (commonly found on graphitized carbon black), and their molecular parameters are taken from the OPLS set (Jorgensen, 1984, 1986).

### 2.3 Isotheric Heat of adsorption

The isotheric heat at zero loading is calculated from (Do *et al.*, 2008)

$$q_{st,ex}^{(0)} = kT - kT \frac{\int_{\Omega} \int_{\omega} [\phi(\mathbf{r}, \omega) / kT] \exp[-\phi(\mathbf{r}, \omega) / kT] d\mathbf{r} d\omega}{\int_{\omega} \int_{\Omega} \exp[-\phi(\mathbf{r}, \omega) / kT] d\mathbf{r} d\omega - V_{acc}} \quad (17)$$

## 2.4 Adsorbent Model

The model for GTCB with functional groups was proposed by Nguyen *et al.* (2014) and is briefly described here. The graphene consists of two parallel layers, each of 2800 carbon atoms arranged in tessellated hexagons (with a spacing of 0.142nm between the carbons) with *x*- and *y*-dimensions of 8.61nm × 8.52nm. 23 functional groups were then added at the edge sites of each graphene sheet so that the separation between two adjacent groups in each layer was approximately 1.23nm, and the functional groups in the 2<sup>nd</sup> layer were offset with those of the 1<sup>st</sup> layer. Finally the model solid was constructed from 15 graphene layers, by the addition of a further 13 layers which were replicas of the first two layers. A number of functional groups were then removed at random to leave a remaining 250 phenol groups. This procedure gives the same O/C ratio as reported by Larsen *et al.* (2012) who used XPS to determine the oxygen content of a series of carbon blacks (CB) and found a ratio of 0.005 for CB heat-treated at 3000°C.

## 3. Experiments

Experiments were performed with the highly graphitized thermal carbon black, Carbo-pack F, supplied by Supelco, USA (*BET* area = 4.9m<sup>2</sup>). Its *TEM* image of Carbo-pack F was reported in Nguyen *et al.* (2013) and Horikawa *et al.* (2015), and it shows the multi-facets of the basal plane composed of graphene layers. Similar image was also reported for P-33 (Graham and Kay, 1961), which was known as the most homogeneous graphitized carbon black, for comparison. Recent results of *SEM* and *TEM* (Yoshizawa *et al.*, 2006, 2008, 2010) also show the polyhedron shape of particles of carbon black graphitized at temperatures greater than 2500C. Our *XPS* study has shown that Carbo-pack F contains oxygen groups (in agreement with the work of Larsen *et al.*, 2012), and the most probable location is at the junctions of the two adjacent basal planes where the edge sites will be exposed.

The graphitization temperature and surface areas of other *GTCBs* analysed in this work, are listed in Table 1.

**Table 1:** BET area and crystallite size of various GTCBs

Carbon black	Graphitization Temperature (C)	BET area (m <sup>2</sup> /g)	Crystal size	Reference
Spheron 6  (known as Graphon)	none	114	25nm	Rouquerol <i>et al.</i> (2013) Carrott <i>et al.</i> (1987) Sing <i>et al.</i> (1994)
	1000	91		
	1500	88		
	2000	85.4		
	2700	84.1		
Sterling FT  (known as P-33)	none	15.5		Deitz (1967)
	1000	13.1		
	1500	12.9		
	2000	12.6		
	2700	12.5	200nm	
Sterling MT	3100	6 - 8	500nm	Gale and Beebe (1964)
Carbopack F	3000	4.9	500nm	This work
GTCB (Dubinin)	3000	28.9		Berezkina <i>et al.</i> (1969)
NC-1 (graphite)	-	4		Pierce and Smith (1950)

No matter how graphitization was carried out, graphitized carbon black, always retains a small residue of functional groups. Using water and methanol as molecular probes, we have developed a method to estimate the low concentration of functional groups in Carbopack F as  $5 \times 10^{-8}$  mol/g (Nguyen *et al.*, 2014; Zeng *et al.*, 2015), which is in the same order as that determined by Bruner *et al.* (1976) for Sterling FT(2700) and Carbopack C(2700). From the BET area (4.9m<sup>2</sup>/g) of Carbopack F and a projection area for the functional group of 0.1nm<sup>2</sup> we find that the fraction of the area occupied by these groups is 0.06%, which is in good agreement with the results of Young *et al.* (1954) obtained from heat of immersion data. Other evidence also points to the existence of residual functional groups on the surface of graphitized carbon black, for example: Campanella *et al.* (1982), Bruner *et al.* (1976), Zettlemoyer (1968), Smith *et al.* (1956) and Healey *et al.* (1955).

### 3.1. Measurements of Adsorption Isotherms

High-resolution isotherms for adsorption on Carbopack F were measured using a volumetric adsorption apparatus (BELSORP-max, supplied by MicrotracBEL, Osaka, Japan). To clean its surface, the sample was heated to 473K for 5h under vacuum at pressures of less than 0.1mPa until the leak rate was less than  $5 \times 10^{-3}$  Pa/min.

## 4. Results and Discussion

### 4.1 Argon and Nitrogen on graphite

Adsorption on *GTCBs* has been extensively studied in earlier work since its very homogeneous surface can be used to probe the gas-solid interaction at a fundamental level. Early heat of adsorption experiments for nitrogen on various carbon blacks, were carried out by Beebe and co-workers in 1947. The un-graphitized surfaces of these carbons were reflected in the continuously decreasing heat of adsorption versus loading (i.e. adsorption occurs on progressively weaker sites as loading is increased; shown as a dashed line in Figure 3a). The strong sites are most probably due to fine crevices in these un-graphitized samples which are in effect ultra micropores, where overlap of adsorbent potential energy from opposite surfaces produces very deep potential energy wells. The heat of adsorption at zero loading of 17.6kJ/mol can be compared with its value on a highly graphitized carbon black of 8.8kJ/mol (in good agreement with the theoretical calculation of 9kJ/mol; Do *et al.*, 2008) and accords closely with the expected doubling in the heat of adsorption in slit pores that can accommodate one layer of molecules (Everett and Powl, 1976).

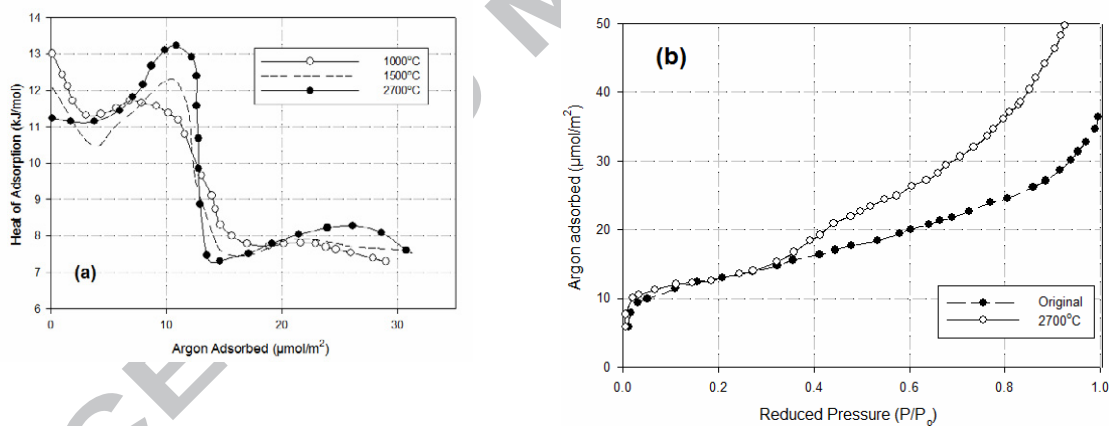


**Figure 3:** (a) Evolution of the isosteric heat of nitrogen versus graphitization for Spheron 6 (data taken from Beebe *et al.*, 1953, 1954; Pace *et al.*, 1957, 1959); (b) Evolution of nitrogen isotherms at 77K for Spheron 6 with the graphitization temperature (data taken from Polley *et al.*, 1953).

After graphitization at high temperatures (greater than 2700<sup>0</sup>C) Spheron 6 is known as Graphon, and the adsorption isotherms and isosteric heats change. Polley *et al.* (1953) demonstrated the evolution of the isotherms with the degree of graphitization; their isotherms (Figure 3b) show the development of waves with increasing graphitization which approach the stepped (Type VI) isotherms found on exfoliated graphite and attributed to discrete

adsorbate layer formation. The corresponding isosteric heat curves, shown in Figure 3a, have a decaying oscillating pattern, which again is typical for simple gases on a homogeneous surface (Beebe and co-workers, 1953, 1954; Bobka *et al.* (1957); Pace *et al.* (1960); Ross and Pultz, 1958) except at very low loadings where the presence of very small quantities of very strong sites (ultra-micropores) affects the heat. The isosteric heat at zero loading for the basal plane can be obtained by extrapolating the linear section in the sub-monolayer region to zero loading, and it is a measure of the intrinsic interaction between an adsorbate molecule and the graphene basal planes. The heat increases almost linearly in the monolayer region, resulting from the increase in the number of neighbouring adsorbate molecules, and reaches a maximum at loading close to the monolayer coverage concentration. Beyond this, the heat decreases because molecules adsorbed in the second layer are further away from the surface and experience a weaker adsorbent field. The second weaker heat maximum is due to the increasing number of neighbouring molecules in the second layer, and further weaker maxima occur as molecules are added to higher layers.

The interesting behaviour of argon and nitrogen on graphene surfaces was further studied by Ross and co-workers (1955, 1958) on the highly graphitized carbon black P33 (*BET* area of  $12\text{m}^2/\text{g}$ ; also known as Sterling FT-2700) shown in Figure 4a. In their data at very low pressure in the sub-monolayer region the surface Henry constant ( $K_A$ ) for argon at 77K was determined as  $4.2 \times 10^4 \text{nm}$ , which is in good agreement with the theoretical value calculated from eq.(14a) as  $4.21 \times 10^4 \text{nm}$  for a homogeneous graphitized surface. Our experimental results for argon on highly graphitized Carbopack F at 77K and 87K (Figure 4b) give Henry constants of  $4.2 \times 10^4 \text{nm}$  and  $1.1 \times 10^4 \text{nm}$ , which are also in perfect agreement with the theoretically calculated values of  $4.21 \times 10^4 \text{nm}$  and  $1.2 \times 10^4 \text{nm}$ , respectively. We particularly note the small upward bend of the isotherm at low pressures, which is evidence that the increasing fluid-fluid interactions in the first layer, neglected in the Langmuir and BET theories, are also responsible for the increase of heat in this region. At sufficiently low temperatures (typically below the bulk triple point), there is a 2D-transition in the first layer and this was observed experimentally by Larher (1978) on exfoliated graphite, and confirmed by the computer simulation studies of Nguyen *et al.* (2010). This is clear evidence that simple gases, such as argon and nitrogen, adsorb by molecular layering on the basal plane of *GTGB*. Other gases such as methane, ethylene and sulphur hexafluoride also follow this mechanism of adsorption (Avgul and Kiselev, 1970). Another feature of the 2D-transition is



the constant heat of adsorption across the transition. This has been reported for the adsorption of carbon tetrachloride and ethyl-chloride (Avgul and Kiselev, 1970), and later confirmed by computer simulation (Do *et al.*, 2008; Nguyen *et al.*, 2010).

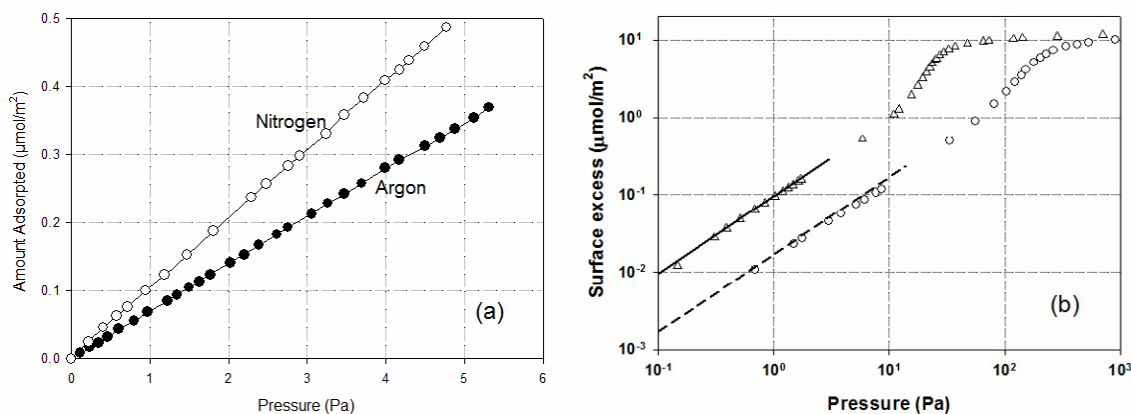


**Figure 4:** (a) Experimental adsorption isotherms for argon and nitrogen at 77K on Sterling FT(2700) at very low loadings (taken from Ross *et al.*, 1955, 1958); (b) Experimental isotherms for argon at 77K and 87K (points) on Carbpac F and theoretical calculations (lines: Do *et al.*, 2008; Nguyen *et al.*, 2013)

Our work on adsorption of water and methanol and XPS studies (Nguyen *et al.*, 2013; Zeng *et al.*, 2015) on *GTCB* indicate that the surface also has a very small quantity of strong sites which strongly favour the adsorption of associating fluids. The question of an initial adsorption of argon or nitrogen on the functional groups or strong sites prior to the adsorption on the basal plane was resolved by the experiments carried out by Dubinin and co-workers in 1969. They measured the adsorption of argon on *GTCB* graphitized at 3000<sup>0</sup>C with a *BET* area of 28.9m<sup>2</sup>/g and showed that the adsorption isotherms of argon and nitrogen on *GTCB*, preloaded with a quantity of water equivalent to a monolayer coverage, were practically the same as those on a clean *GTCB* surface (see Figure 5). This demonstrates that argon and nitrogen adsorb predominantly on the basal plane, and that water adsorbs predominantly on the functional groups and/or strong sites such as defects grafted at the unsaturated locations at the edges of the graphene layers.

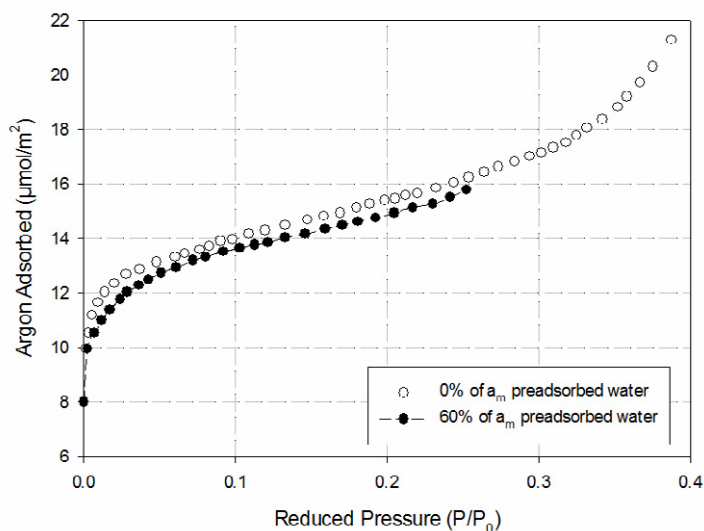


**Figure 5:** Adsorption of argon on a carbon black graphitized at 3000 C pre-loaded with water whose amount is equivalent to 0% and 60% of the monolayer coverage of water (data taken from Berezkina *et al.*, 1969)

To substantiate this argument, we show in Figure 6 the Henry constant as a function of temperature for various adsorbates on the basal plane (Figures 6a, b) and on a single carboxylic functional group (Figure 6c). At 87K for example, the theoretical Henry constant for argon on the basal plane is  $1.2 \times 10^4 \text{ nm}^3$  (eq. 14a) and the Henry constant for argon on a carboxylic group is  $1.3 \text{ nm}^3$  (eq.15). Taking the estimated concentration of the carboxylic functional group on the Carbopack F as  $0.00005 \text{ mmol/g}$  (Zeng *et al.*, 2015) and the *BET* area of  $4.9 \text{ m}^2/\text{g}$ , we find that the Henry constant for argon adsorption on the basal plane is much greater (more than 1 million times) than that on the functional group. Therefore adsorption of argon on *GTCB* is dominated by adsorption on the basal plane surface, unless the graphitized carbon black has fine crevices in large quantity. Experimental data of Lopez *et al.* (1961) with mineralogical graphite shows that there are two Henry constants, the second of which agrees with the theoretical Henry constant on the basal plane of graphite. Therefore the first Henry constant must be due to the fine crevices and they contribute only to very small capacity, typically around 0.1% of the monolayer coverage. Our preliminary simulation shows that a typical crevice will have a pore width of around 0.65-0.7nm (distance between the centre of carbon on one wall to the corresponding centre of the opposite wall). Details of this analysis will be reported in future communication.

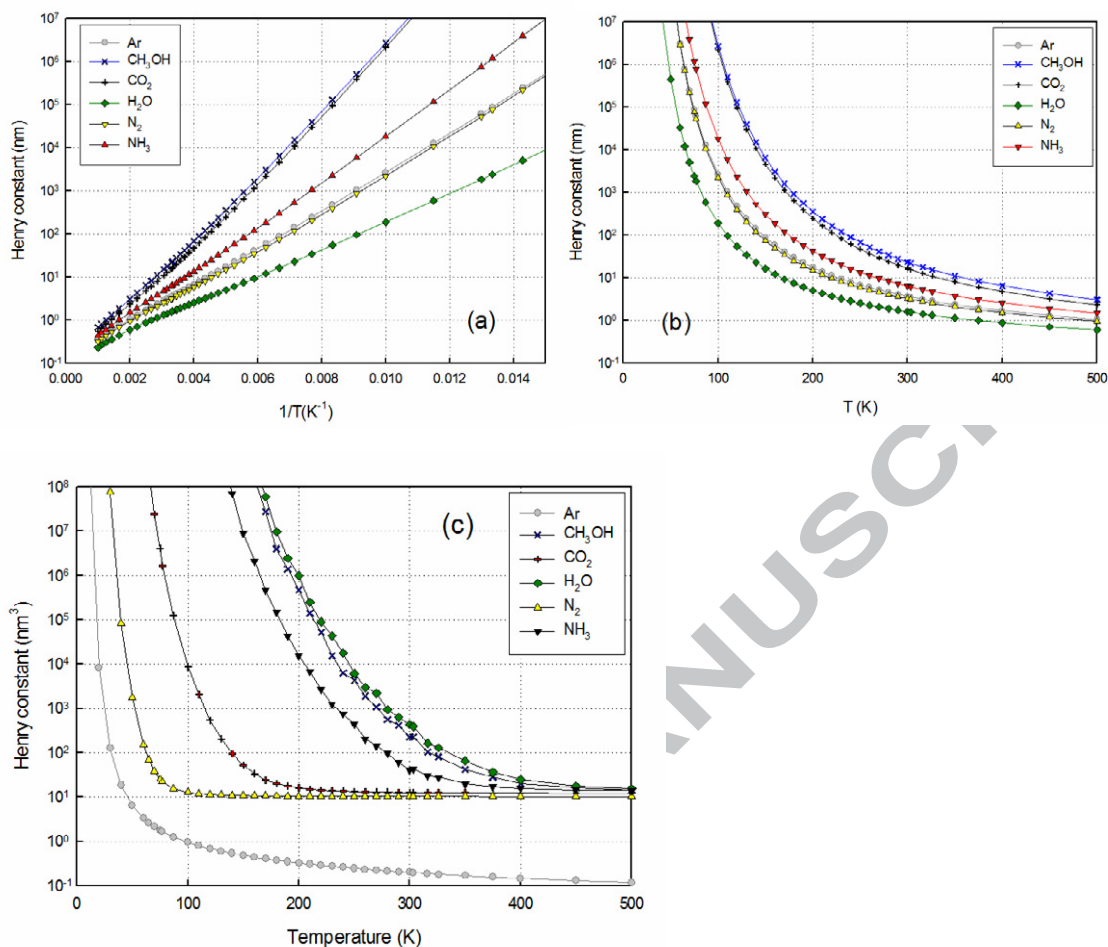


**Figure 6:** Theoretical Henry constants of various gases (a) and (b) graphene layer, (c) functional group

Because the early calorimetric measurements for argon adsorption made by Beebe, Pace, Kington and their co-workers were made by discrete, rather than by continuous, methods they did not observe the small jump in the density in the monolayer region nor the spike close to monolayer completion in the plot of the isosteric heat versus loading. Two decades after these earlier studies, Rouquerol and co-workers, in 1977 developed a quasi-equilibrium technique by which the data could be continuously recorded on a chart recorder, and detected the subtle small substep in the isotherm and a spike in the heat curve versus loading, and subsequently further extended by Grillet *et al.* in 1979, for adsorption of argon and nitrogen at 77K on Sterling MT(3100) whose *BET* area is 7.8m<sup>2</sup>/g. With the exception of the spike, their heat curves agree well with those of Beebe and co-workers (Figure 3). The small step in

the isotherm and the spike in the heat curve only occur when the adsorption takes place on an energetically homogeneous surface.

The isotherms and the isosteric heat, especially the heat spike observed by Rouquerol *et al.*, were reproduced successfully by the molecular simulations of Do and co-workers using the Bin-Monte Carlo and kinetic Monte Carlo techniques (Fan *et al.*, 2011; Nguyen *et al.*, 2011; Ustinov and Do, 2012).

The above evidence points clearly to the fact that beyond a very small initial adsorption, simple gases adsorb on the basal planes of the poly-crystallite of *GTCB* by molecular layering, for at least the first two layers. For higher layers layering becomes more disordered because of thermal fluctuations and the decay of the ordering effect due to the solid-fluid potential.

Many other experimental adsorption studies of simple gas adsorption on *GTCB* have been reported, amongst which may be mentioned those of Isirikyan and Kiselev (1962); Sarakhov *et al.* (1961, 1963); Berezkina *et al.* (1969); Kruk *et al.* (1999); and Gardner *et al.* (2000) who have also reproduced experimental results by simulation and density functional calculations.

#### 4.2 CO<sub>2</sub> adsorption

Clearly the adsorption on *GTCB* of argon and nitrogen, despite its weak quadrupole moment, is predominantly a molecular layering onto the basal plane. CO<sub>2</sub> is commonly used as an adsorbate for characterization; it has a larger quadrupole moment than nitrogen and therefore there may be a contribution to the initial adsorption from electrostatic interaction with functional groups. Adsorption isotherms and an isosteric heat curve for CO<sub>2</sub> on *GTCB* at 194K were first reported by Spencer *et al.* in 1958. These are shown in Figure 7. The trends are similar to those observed earlier for argon and nitrogen, and indicate a molecular layering mechanism, as confirmed by the computer simulations of Do and Do in 2006. The ratio of the theoretical Henry constant for the basal plane to that of the functional group is 384, thus favouring adsorption on the basal plane over the functional group. Furthermore the area of the functional groups is much less than that of the basal plane, and therefore adsorption on the functional groups was not detected.

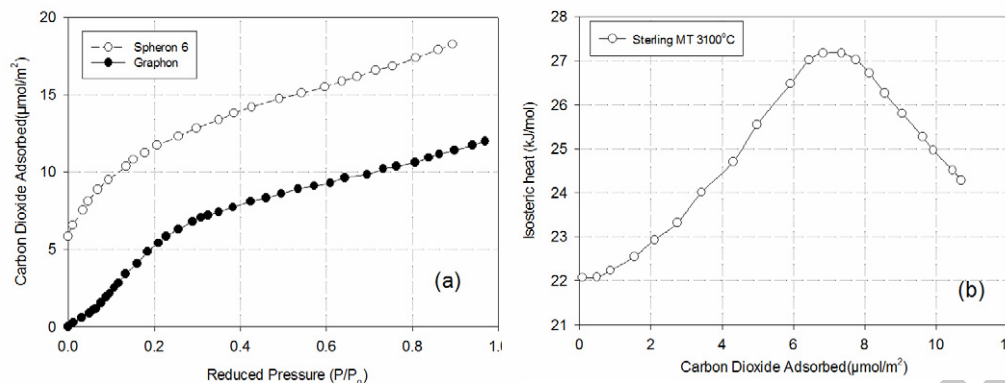


**Figure 7:** (a) Adsorption isotherm of carbon dioxide on un-graphitized Spheron 6 and Graphon at 194K (Data of Spencer *et al.*, 1958); (b) Isothermic heat versus loading for Sterling MT(3100) from the data of Spencer *et al.*, 1958.

In an effort to look for evidence of strong sites on *GTCB*, Deitz (1967) carried out experiments at higher temperatures than Spencer and co-workers, where the Henry law region is shifted to higher pressure and the data can be measured with better precision. For the adsorption of  $\text{CO}_2$  on Sterling FT(2700) at 273K, he observed a two stage uptake at extremely low pressure, which is evidence of two independent sites for adsorption (Figure 8). The first could be due, either to adsorption in defects (fine crevices), or adsorption on functional groups that interact strongly with carbon dioxide via electrostatic interactions. However, Deitz attributed the substantial difference in site energies to strong interaction between the anisotropically polarizable  $\text{CO}_2$  and the anisotropic polarizability of the graphitic surface which has the consequence that the dispersion constant at the edges is much larger than on the basal planes and interpreted his results with the aid of a dual site Langmuir model. As discussed above, the existence of exposed edge sites implies that micropore crevices and functional groups are also likely to be found at the same location (conjunction of graphitic basal planes) so that more than one factor may contribute to the strong interactions. If we assume that the strong sites are solely due to functional groups, and make the assumption that the concentration of the functional groups is the same as that determined for Carbopack F (Zeng *et al.*, 2015), we find that the Henry constant due to the functional groups alone is far too low to explain the experimental Henry result from the data at pressures less than 0.01Pa in Figure 8 which argues for the presence of ultra-fine pores with exposed edge sites in their Sterling FT(2700). To summarise; a two stage adsorption process for carbon dioxide on Sterling FT(2700), is supported by:

1. The two stage uptake observed by Dietz when for samples heated to 750C.

- The isosteric heat versus loading curves of Spencer *et al.* (1958) for Sterling FT(2700) which show a high initial heat (first stage), followed by a decrease and then a linear increase with loading in the monolayer region (second stage).
- The second stage isotherm and isosteric heat data have been confirmed by the computer simulations of Do and Do (2006) for carbon dioxide adsorption on a pure graphene surface.

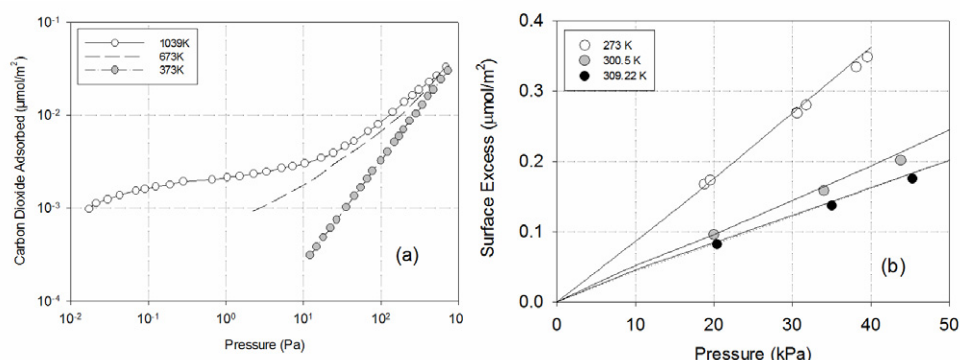


**Figure 8:** (a) Adsorption isotherm of carbon dioxide at 273K on Sterling FT(2700) from the data of Deitz (1967). The temperatures on the curves are the different outgassing temperatures. (b) Adsorption isotherm of carbon dioxide at 273K, 300K and 309K (data taken from Myers and Prausnitz (1965), on GTCB FT-D3(2800) (BET area of 12m<sup>2</sup>/g), which is the same as the P-33 (2700)

The data of Spencer *et al.* miss this two stage process because at 194K, adsorption on the strong sites occurs at very low pressures which were outside the range of their instruments.

Adsorption of carbon dioxide at low pressure was measured by Myers and Prausnitz (1965) at 273, 300 and 309 K (Figure 8b), but since their data were not extended to extremely low pressure, their Henry constants at these temperatures agree well with the theoretical Henry constant for a basal plane surface of graphite, but do not detect the higher values found by Deitz which we attribute to the presence of strong sites. For example at 273 K Myers and Prausnitz found an experimental Henry constant of 27 nm, compared to the theoretical value, calculated from eq. 14a, of 29 nm.

#### 4.3 Methanol adsorption

The OPLS model for methanol has partial charges of  $\sim -0.7e$  on the oxygen, rather smaller than in water ( $\sim -0.84e$ ), and the compensating positive charge is distributed between the OH group hydrogen and the methyl group (Appendix 1); so compared to water, only a moderate degree of hydrogen bonding can occur. The average intermolecular potential energy between two methanol molecules is stronger than between two CO<sub>2</sub> at similar separations because,

although the electrostatic interactions are similar, the  $\epsilon/k$  assigned to the  $\text{CH}_3$  group is higher than that for O or C in  $\text{CO}_2$ . The earliest reported experimental data for methanol adsorption on *GTCB* is that of Pierce and co-workers in 1950, who studied adsorption of methanol on graphite NC-1 and Graphon (Figure 9a). The former has structural defects in the form of pores and therefore only the data on Graphon is indicative of methanol adsorption on a homogeneous graphitic adsorbent with strong sites at the edges of the graphene layers.

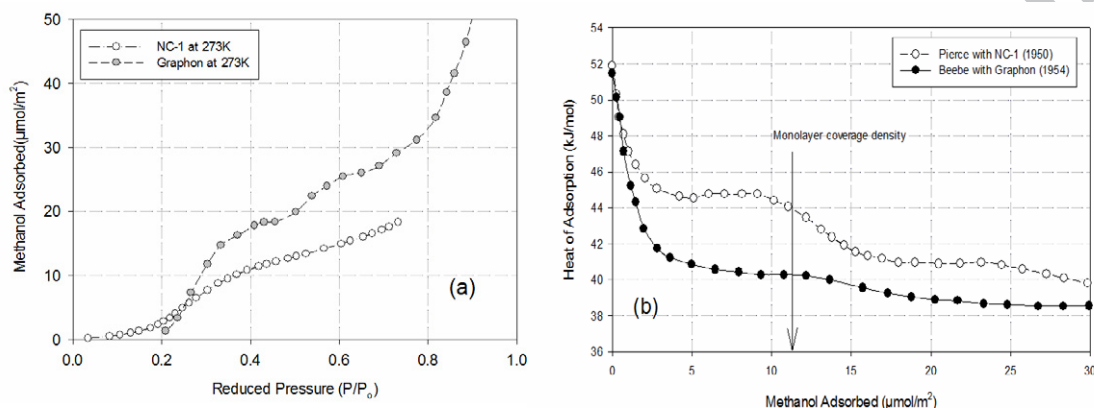


**Figure 9:** (a) Adsorption isotherm of methanol on Graphon and graphite NC-1 at 273K (data taken from Pierce and Smith, 1950); (b) Isotheric heat of methanol on graphite NC-1 (data of Pierce and Smith, 1950) and on Graphon (data of Millard *et al.*, 1954)

Subsequently a study of methanol adsorption on Graphon was carried out by Millard *et al.* (1954), and similar results were obtained (Figure 9b). The effects of adsorption temperature, depicted in Figure 10, are from the experiments of Belyakova *et al.* (1968), and were later shown to be in good agreement with computer simulations (Nguyen *et al.*, 2013).

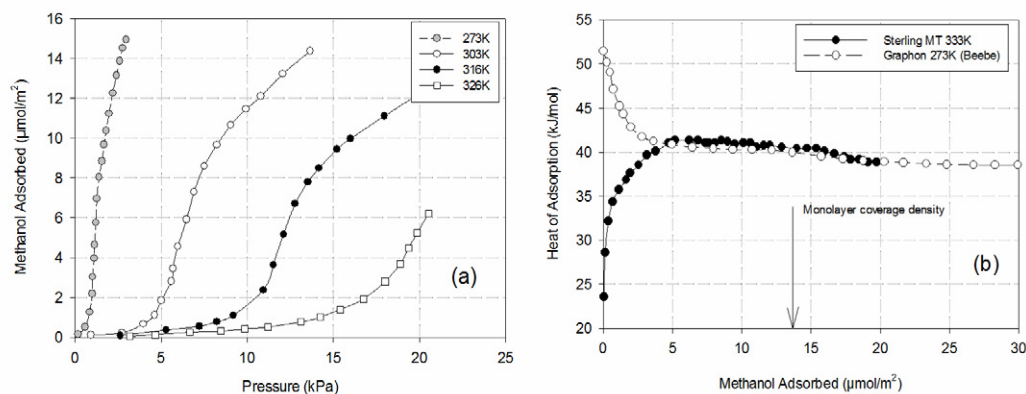


**Figure 10:** (a) Adsorption isotherms of methanol on Sterling MT(3100) at various temperatures (data taken from Belyakova *et al.*, 1968); (b) Isotheric heat of adsorption on Graphon (data of Millard *et al.*, 1954) and on Sterling MT(3100) (data of Belyakova *et al.*, 1968).

In the data of Pierce, Beebe and Kiselev and their co-workers there is hardly any adsorption at reduced pressures below 0.2; adsorption begins above this pressure and rises to a plateau at a reduced pressure of 0.4, corresponding to the formation of a monolayer of methanol. Further increase in pressure results in the formation of multilayers on the carbon surface.

The isosteric heat on Graphon is very high at zero loading, decreases quite steeply in the sub-monolayer region and approaches a plateau at a loading of about one third of the monolayer coverage (Figure 10b). This plateau extends until the first layer has been completed, and then the isosteric heat decreases because adsorption begins in the second and higher layers. This isosteric heat pattern for methanol adsorption can be interpreted as follows.

1. The initial adsorption occurs at the strong sites (functional groups and/or ultra-fine crevices) to form an adsorbed complex, which then forms an anchor for methanol molecules to adsorb around it to form clusters.
2. As the clusters grow, methanol starts to spill over onto the basal plane, favoured by the interaction of incoming methanol molecules with the clusters as well as their interaction with the basal plane via the methyl group. The consequence is a constant heat in the sub-monolayer region, in marked contrast to the rising heat curves for argon, nitrogen and carbon dioxide.

We suggest that this spill-over mechanism in physical adsorption is a plausible explanation of the phenomena observed for methanol adsorption on GTCB. As far as we are aware this is the first time that this mechanism has been put forward in the literature. We summarize the mechanism visually in Figure 11.

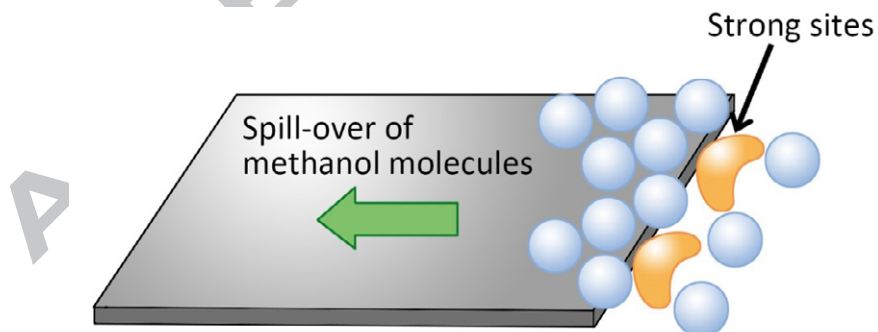


**Figure 11.** Schematic description of the adsorption mechanism of methanol on GTCB



The proposed mechanism is supported by the values of the theoretical Henry constants, on the basal plane and on the functional group, of 23nm and 1.5nm, respectively. So any strong sites that are detected experimentally must include defects along the edges of the basal plane of graphene layers. Our own experimental data (Figure 12) show that the initial Henry constant at 273K is at least 3500nm, which we interpret as evidence for the presence of fine crevices. Even in the second stage, the Henry constant is 300nm, which is much greater than the calculated Henry constant of the basal plane. This can be taken as evidence of clustering at the edge plane that promotes the adsorption on the basal plane.

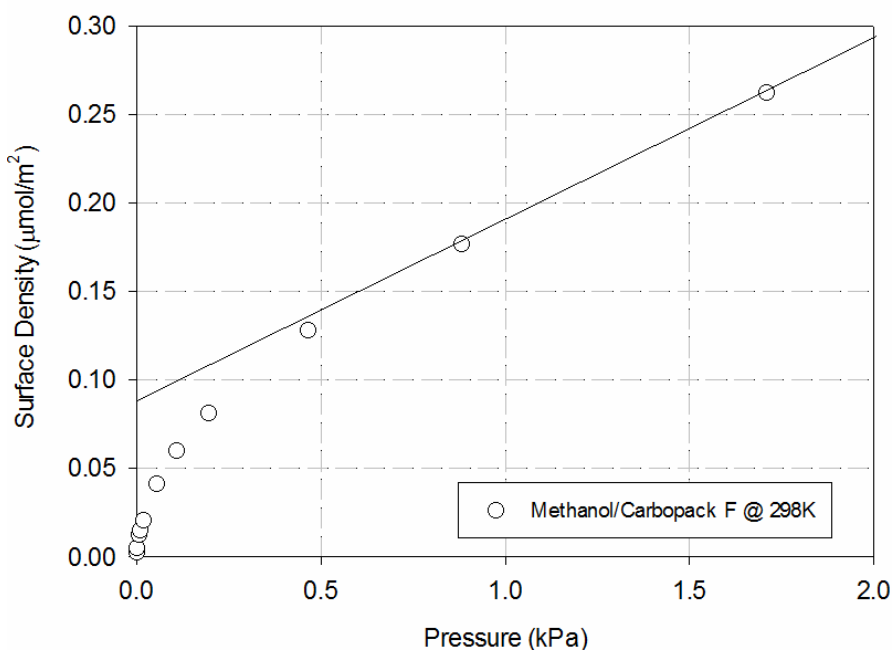


**Figure 12:** Adsorption of methanol on Carbopack F at 298K in the very low pressure region, where the loadings are less than 2% of the monolayer coverage concentration.

#### 4.4 Ammonia adsorption

Hydrogen bonding in ammonia is stronger than in methanol as may be judged from the high partial charge carried by the N atom (Appendix 1). Experimental data for ammonia adsorption on graphite and carbon black is scarce, compared to that for argon or nitrogen. The earliest report is from Smith and Pierce (1948) and Pierce *et al.* (1949) who published an isotherm and heat of adsorption curves for ammonia adsorption on graphite NC-1 at 194K.

This graphite is not homogeneous, but the isotherm is nevertheless of Type III; adsorption begins around a reduced pressure of 0.5, and the isosteric heat decreases continuously with loading. Dell and Beebe in 1955 used Spheron 6 and its graphitized versions to obtain the isotherms and isosteric heat reproduced in Figures 13a and b. The graphitized samples show a steeper onset of adsorption, again at about  $P/P_0 = 0.5$  as observed earlier by Pierce *et al.* Like methanol, the heat curve has a steep initial decrease with loading, denoting the presence of strong sites. Also in common with methanol, there is a constant heat plateau in the sub-monolayer region. These features seem to support the notion of a spill-over phenomenon but one that begins at a higher reduced pressure than methanol because the methyl group in methanol interacts more strongly with the basal plane of graphene than does the nitrogen atom in ammonia.

In their further, more refined, study Holmes and Beebe (1957); Spencer *et al.* (1958); Beebe *et al.* (1964) extended their work to Sterling MT(3000)<sup>1</sup>, which had also been treated with hydrogen at high temperatures to reduce the quantity of functional groups, and therefore is more homogeneous than the Graphon previously studied. Their isotherm is reproduced in Figure 13c and again there is negligible adsorption at reduced pressures less than 0.5, and a very sharp onset of adsorption at 0.5. In contrast to the other adsorbates discussed so far (for example the reversible nitrogen isotherm on the same adsorbent illustrated in Figure 13c) the isotherm has a hysteresis loop which only closes at very low pressure which we attribute to the strong intermolecular attraction between ammonia molecules. Hysteresis may therefore be expected for adsorbates that have strong FF interactions, for example water, as we will show next. Data on acetone and  $\text{CH}_2\text{Cl}_2$  on highly graphitized carbon black also show hysteresis (Kruchten *et al.*, 2003; Volkmann *et al.*, 1993), as further evidence that strong interactions between adsorbate molecules is responsible for the observed hysteresis loop.

---

<sup>1</sup> BET area of  $6.3\text{m}^2/\text{g}$  and a microcrystal size of 500nm.

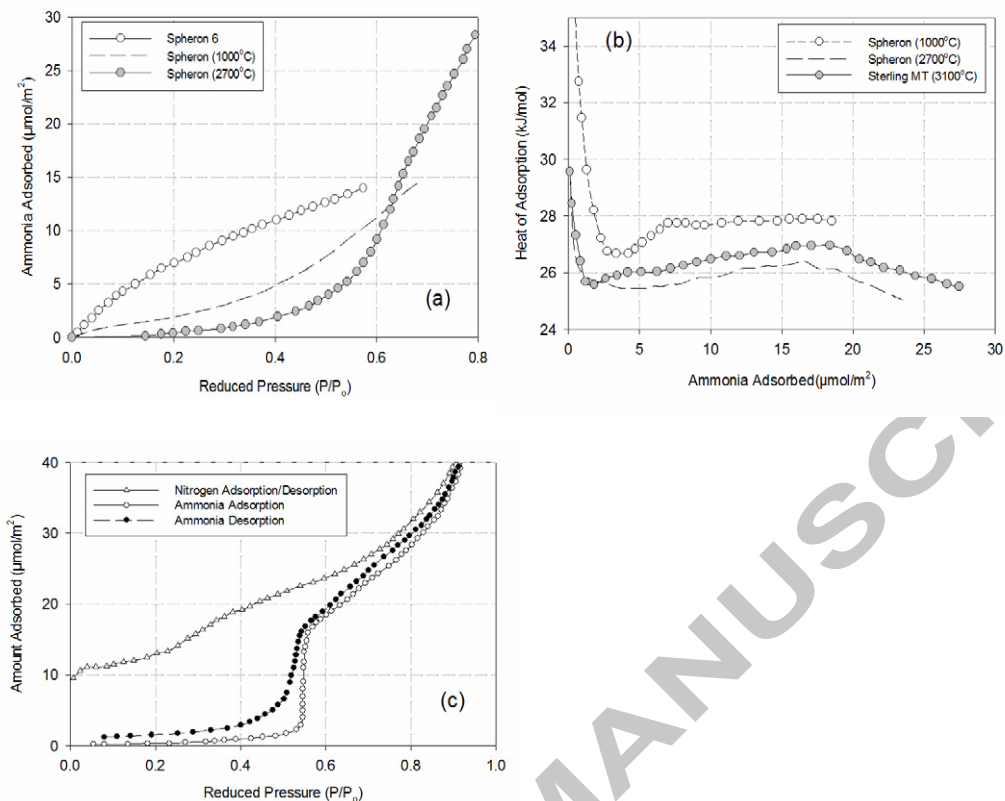


**Figure 13:** (a) Adsorption isotherms of ammonia on Spheron 6 at different graphitization temperatures; (b) Isotheric heat versus loading for Spheron 6(1000), Spheron 6(2700) and Sterling MT(3100); (c) Hysteresis in ammonia adsorption (symbols) at 194K on Sterling MT(3100) and the reversible nitrogen isotherm (line) at 77K on the same sample.

The heat of adsorption curve for ammonia on Sterling MT(3100) is essentially the same as that for Spheron (2700) (Figure 13b), and is further evidence of spill-over as suggested as an interpretation of the methanol data.

Figure 14 shows the experimental data of ammonia on Vulcan III (a *GTCB*) from the work of Bomchil *et al.* (1979), and displays two Henry constants: the first can't be determined because the low pressure data is insufficient to be able to make an accurate determination. The second Henry constant from the slope of the second linear part of the isotherm is 635nm, which is an order of magnitude larger than the theoretical Henry constant for ammonia on the basal plane of graphite of 60nm. An explanation for the difference between the experimental and theoretical values is the strong interactions with the clusters around the low energy sites. Although the Henry constant for these sites is not directly accessible experimentally, we can calculate the theoretical Henry constant contributed by the functional group by assuming that

the concentration of a carboxylic group is  $5 \times 10^{-8}$  mol/g (as determined for our Carbopack F (Zeng *et al.*, 2015); we estimate this to be 250nm. This is still considerably less than the Henry constant estimated from the data of Bomchil *et al.*, but some of the discrepancy could be attributed to the fine crevices at the edges of graphene layers which can account for as much as a factor of 2 arising from potential energy overlap. In addition, the anisotropy factor discussed by Meyer and Deitz (1967), and invoked by Deitz (1967) as a reason for the strong adsorption of CO<sub>2</sub> would also play a part in ammonia adsorption.

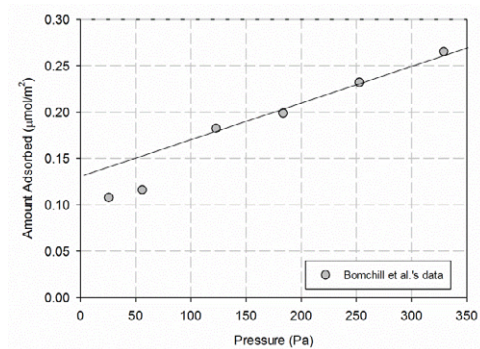


**Figure 14:** Adsorption isotherm of ammonia on Vulcan III at 191K (data taken from Bomchil *et al.*, 1979)

#### 4.5 Water adsorption

Water is, perhaps, the most fascinating adsorbate to study because of its unique properties (many of its interesting properties are detailed in a website by Chaplin) and ubiquitous occurrence as a component in many adsorbates. Its essential character originates from the very strong hydrogen bonding, due to the exceptionally high partial charges on H and on the O lone pair (Appendix 1). There is a vast number of adsorption studies of water in porous carbons because of its many practical applications in environmental areas and catalysis (Juhola and Wiig, 1949; Brennan *et al.*, 2001). The first investigation of water adsorption on carbon black was made by Emmett and co-workers in 1945, and their isotherms for water on un-graphitized Spheron 6 are reproduced in Figure 15a. The isotherm shows the onset of adsorption at a reduced pressure of around 0.5. Unlike the adsorption of ammonia on highly graphitized Sterling MT(3100) the adsorption here, on un-graphitized Spheron 6, is in micropores as the amount adsorbed correlates well with the micropore volume, and the hysteresis loop in carbon micropores is due to the re-orientation of water molecules as adsorption proceeds which makes the adsorbed phase more cohesive and thus desorption is delayed until low pressures are reached.

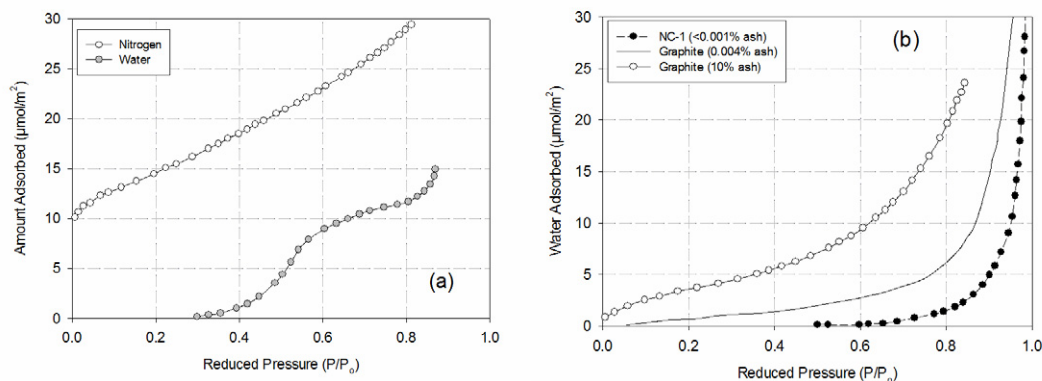


**Figure 15:** (a) Adsorption of nitrogen at 77K and water at 303K on ungraphitized Spheron 6 (Data of Emmett and Anderson, 1945); (b) Effects of ash content on the water adsorption on graphite (data of Harkins and Jura, 1946) and on NC-1 (data of Pierce *et al.*, 1949)

Harkins and co-workers (1946) and Pierce and co-workers (1949) studied water adsorption on (presumably) non-porous graphite and found that the isotherms were typical of those expected for graphitized carbon (Figure 15b). The distinction between adsorption on a surface and in a pore can be seen at the onset of adsorption which, for a highly graphitized surface, does not occur until the pressure is close to the saturation vapour pressure (or even beyond, Easton and Machin, 2000). By contrast, adsorption in porous carbons begins at a lower pressure, which can be attributed either to the larger concentration of functional groups or to the nucleation of clusters from water trapped in very small pores (Nguyen and Bhatia, 2011) and the ease with which clusters can grow and merge due to the proximity of the pore walls (Emmett *et al.*, 1948).

Pierce, Smith and co-workers (1950, 1951), Young *et al.* (1954) and Millard *et al.* (1955) made some of the earliest studies of water adsorption on the graphitized thermal carbon black, Graphon (Figure 16). Naono *et al.* (1997) also used Graphon as an adsorbent and reported similar isotherms. The comparison between the water isotherm for Graphon and graphite NC-1 shows that Graphon is more homogeneous than graphite because of the onset of water adsorption in Graphon occurs at a pressure much closer to the saturation vapour pressure. We also showed in Figure 16 the adsorption isotherm of ammonia to show the different onsets of adsorption of ammonia and water, which reflect the degree of hydrogen bonding: ammonia < water.

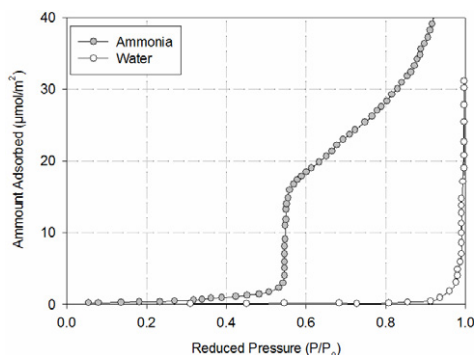


**Figure 16:** Comparison between the adsorption isotherm of ammonia at 194K (Data of Holmes and Beebe, 1957) and water on Graphon (data of Pierce and Smith, 1950)

The role played by functional groups in water adsorption on carbon black and graphite is very important. The effects of functional groups were studied by Pierce *et al.* in 1951 and Healey *et al.* in 1955 (Figure 17) and by Belyakova *et al.* (1968). The isotherms from these papers are all of Type III, but the heat of adsorption varies qualitatively depending on the extent of graphitization of the carbon black. For example, Kiselev and co-workers reported a low value for the heat at zero loading, an increase in the region of the sub-monolayer; the heat then remains constant over the monolayer region. On the other hand, Millard *et al.* (1955) observed a constant heat over the complete range of pressure for water adsorption on Graphon but a decreasing trend on un-graphitized Spheron 6. Miura and Morimoto (1986) reported a variety of types of heat curve (Figure 18). However, it is interesting to note that a common feature is that the heat remains constant in the sub-monolayer region, except in the initial stage, where the gradient of the curve depends on the extent of graphitization. This result is in qualitative agreement with those of Kiselev, Millard and their co-workers.

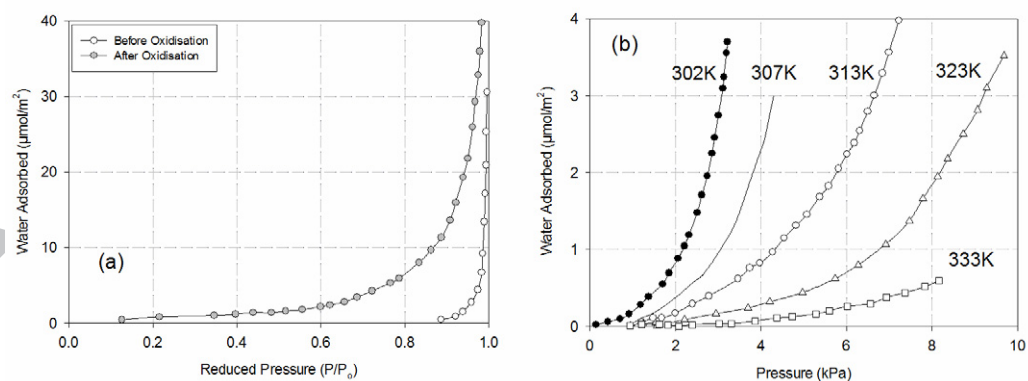


**Figure 17:** (a) Effects of oxidation on water adsorption on Graphon (Data of Pierce and Smith, 1950), and effects of temperature on water adsorption on graphitized carbon black (Data of Belyakova *et al.*, 1968)

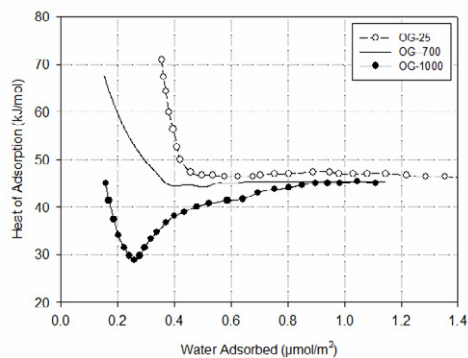


**Figure 18:** Isothermic heat versus loading for graphitized carbon black with different heat treatment (Data of Morimoto and Miura, 1986).

The adsorption isotherms and heats of adsorption for water adsorption when compared with data for other adsorbates suggest the following mechanism for water (Figure 19).

1. Initial adsorption occurs at the functional groups or any strong sites, such as fine crevices (Nguyen and Bhatia, 2011)
2. Water forms clusters around the functional groups and/or fine crevices and the clusters are extended in a direction, away from the basal planes, by hydrogen bonding between the water molecules, i.e. water does *not* spill over onto the basal plane. This is strongly supported by the nice work of Berezkina, Dubinin and co-workers in 1969 where they observed the same amount of argon adsorption on *GTCB*, irrespective of whether the sample was preloaded with water or not (see Figure 5). On the other hand, when the sample was partially preloaded with methanol the amount of argon adsorbed was reduced, depending on the extent of the methanol loading. The growth of water clusters around functional groups in slit pores in activated carbon fibres has been studied by X-ray diffraction by Ohba and Kaneko (2007).

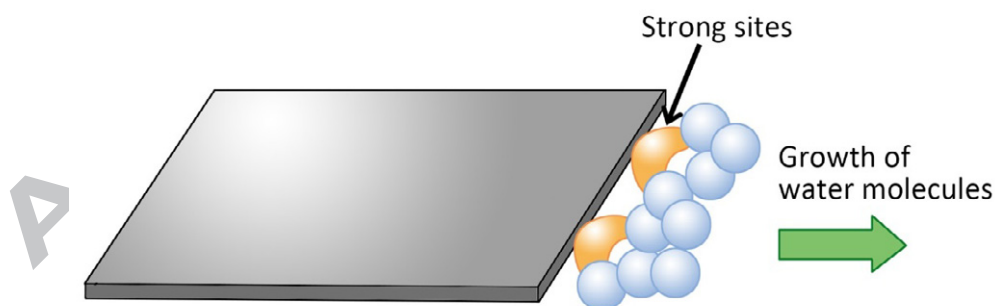
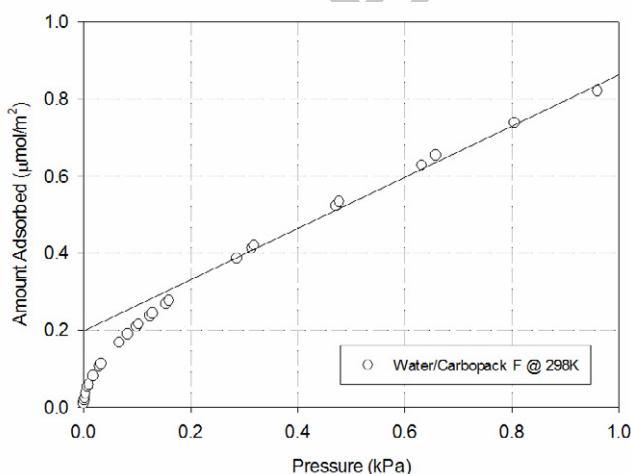


**Figure 19:** . Schematic description of the adsorption mechanism of water on *GTCB*

We have confirmed this mechanism with a new simulation model for water adsorption on *GTCB*. The adsorbent is composed of graphene layers which are grafted with functional groups (Nguyen *et al.*, 2013).

Even though our simulations at ambient temperatures show that water forms a hydrogen-bonded complex with functional groups at the edges of the graphene layers and subsequently grows outward as clusters, without adsorption onto the basal planes, it has been reported that water can wet the basal plane surface at 500K (Zhao, 2007). We are currently investigating this possibility with the above model in the temperature range from 500 to 600 K (the critical temperature of water is 746 K), and will report the results in a future communication.

As further evidence of the importance of the strong sites for water adsorption on *GTCB*, we show in Figure 20, the adsorption isotherm of water on Carbopack F at 298K in the very low pressure region. There is a two stage uptake: the first stage is due to the initial adsorption on strong sites, and the second linear stage is shown as a solid line. The apparent Henry constant from the slope of this line is 1600nm, compared with a theoretical Henry constant for the basal plane of only 1.6nm. This is consistent with our proposed mechanism for water adsorption, i.e. the initial adsorption is around strong sites and the subsequent adsorption occurs by the growth of hydrogen bonded water in clusters, rather than adsorbing onto the basal plane.

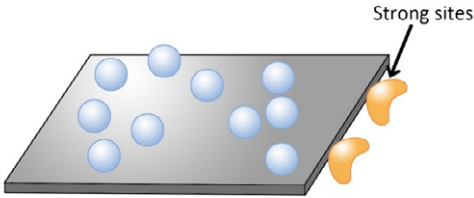
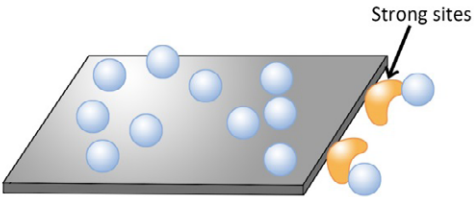
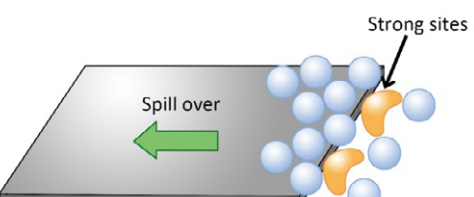
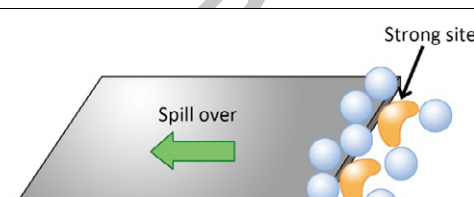



**Figure 20:** Adsorption isotherm of water on Carbopack F at 298K in the very low pressure region.



#### 4. Summary of adsorption mechanism

Here we summarize schematically the proposed adsorption mechanisms for different adsorbates on GTCB. These mechanisms are supported by our recently calculated isosteric heats for a number of adsorbates, ranging from non-polar fluids to polar fluids (Horikawa *et al.*, 2015).

Microscopic configuration	Adsorbate	Section	Ratio of Henry constants of basal plane to functional group
	Argon, nitrogen	4.1	$1.5 \times 10^6$
	Carbon dioxide	4.2	384
	Methanol	4.3	16
	Ammonia	4.4	0.23
	Water	4.5	0.62

The following table summarizes the Henry constants contributed by the basal plane and the functional groups. The calculation is based on a concentration of  $5 \times 10^{-8}$  mol/g for the functional groups.

	Ar @ 87K	CO <sub>2</sub> @ 273K	CH <sub>3</sub> OH @ 300K	NH <sub>3</sub> @ 191K	H <sub>2</sub> O @ 300K
Henry constant by the basal plane (nm)	12,000	30	23	57	1.6
Henry constant by one functional group (nm <sup>3</sup> )	1.3	13	226	42,000	430
C = $5 \times 10^{-8}$ mol/g Henry constant by functional group (nm)	0.0078	0.078	1.4	252	2.58
H(basal)/H(Group)	$1.5 \times 10^6$	384	16	0.23	0.62

## 5 Conclusions

Detailed mechanisms for adsorption on graphitized carbon black, for a number of adsorbates with increasing polarity ranging from argon and nitrogen through to associating fluids such as ammonia and water are presented against the background of experimental evidence and theoretical calculation of Henry constants and computer simulation. Simple gases adsorb primarily by molecular layering, but reveal evidence of high energy sites in the form of crevices at edges or between particles. Adsorbate clustering is the major process for the accumulation of adsorbate of associating fluids. For those adsorbates that form moderately strong hydrogen bonds, we demonstrate that spill-over onto the graphite basal planes links the initial clustering at very low loadings, with spreading and molecular layering as adsorption increases. By contrast water, which is only weakly attracted to the basal planes, but is strongly electrostatic, forms clusters that grow outwards from the graphitic edges and molecular layering does not occur at ambient temperatures.

## References

- Allen, M. P.; Tildesley, D. J. *Computer Simulation of Liquids*; Oxford: Clarendon Press: **1989**
- Avgul, N. N.; Kiselev, A. V. Physical Adsorption of Gases and Vapours on Graphitized Carbon Blacks. *Chem Phys Carbon*. **1970**, *6*, 1 - 124.
- Bandosz, T. J.; Jagiełło, J.; Schwarz, J. A.; Krzyzanowski, A. Effect of Surface Chemistry on Sorption of Water and Methanol on Activated Carbons. *Langmuir*. **1996**, *12*, 6480-6486.
- Beebe, R. A.; Biscoe, J.; Smith, W. R.; Wendell, C. B. Heats of Adsorption on Carbon Black. I. *J Am Chem Soc*. **1947**, *69*, 95-101.
- Beebe, R. A.; Millard, B.; Cynarski, J. Heats of Adsorption of Nitrogen and Argon on Porous and on Non-Porous Carbon Adsorbents at - 195°1. *J Am Chem Soc*. **1953**, *75*, 839-845.
- Beebe, R. A.; Young, D. M. Heats of Adsorption of Argon on a Series of Carbon Blacks Graphitized at Successively Higher Temperatures. *J. Phys. Chem.* **1954**, *58*, 93-96.
- Beebe, R. A.; Kiselev, A.V.; Kovaleva, N.V.; Tyson, R.F.S.; Holmes J.M. Adsorption and State of CO<sub>2</sub>, SF<sub>6</sub>, and NH<sub>3</sub> on the Surface of Graphitized Carbon Black. I. Adsorption Isotherms *Russ J. Phys. Chem*. **1964**, *38*, 372-378.
- Belyakov, L. D.; Kiselev, A. V.; Kovaleva, N. V. Gas-Chromatographic Determination of Isotherms and Heats of Adsorption of Water Benzene and Methanol Vapours on Graphitised Carbon Black. *Russ J Phys Chem+*. **1968**, *42*, 1204-1208.
- Berendsen, H. J. C.; Grigera, J. R.; Straatsma, T. P. The Missing Term in Effective Pair Potentials. *J. Phys. Chem. B*. **1987**, *91*, 6269-6271.
- Berezkina, Y. F.; Dubinin, M. M.; Sarakhov, A. I. Adsorption of Vapors on Model Nonporous Adsorbents with a Physically Modified Surface. *B Acad Sci USSR CH+*. **1969**, *18*, 2495-2501.
- Birkett, G.; Do, D. D. Simulation Study of Water Adsorption on Carbon Black: The Effect of Graphite Water Interaction Strength. *J Phys Chem C* **2007**, *111*, 5735-5742.
- Bobka, R. J.; Dininng, R. E.; Siebert, A. R.; Pace, E. L. Heat Capacity and Heat of Adsorption of Argon Adsorbed on Graphon. *J Phys Chem-US*. **1957**, *61*, 1646-1648.
- Bomchil. 1979. NH<sub>3</sub>. Adsorption. Carbon Black. Structure. *J. Chem. Soc. Farad. Trans. I*. **1979**, *75*, 1535. Harris. Leslie. Tabony. White
- Brennan, J.; Bandosz, T.; Thomson, K.; Gubbins, K. Water in porous carbon. *Colloids & Surf. A*. **2001**, *187-188*, 539-68
- Brunauer, S.; Emmett, P. H.; Teller, E. Adsorption of Gases in Multimolecular Layers. *J Am Chem Soc*. **1938**, *60*, 309 - 319.
- Bruner, F.; Bertoni, G.; Ciccioli, P., Comparison of physical and gas chromatographic properties of Sterling FT and Carbopack C graphitized carbon blacks. *J. Chroma*. **1976**, *120*, 307-19.
- Campanella, L.; Di Corcia, A.; Samperi, R.; Gambacorta, A. The Nature of Surface Chemical Heterogeneities of Graphitized Carbon Black. *Mater Chem*. **1982**, *7*, 429-438.
- Carrott, P.; Roberts, R.; Sing, K. Adsorption of nitrogen by porous and non-porous carbons. *Carbon*. **1987**, *25*, 59-68.
- Cassel, H. M. Cluster Formation and Phase Transitions in the Adsorbed State. *J Phys Chem*. **1944**, *48*, 195-202.
- Chaplin, M. [http://www.lsbu.ac.uk/water/water\\_models.html](http://www.lsbu.ac.uk/water/water_models.html)

- Chen, B.; Potoff, J.; Siepmann, I. Monte Carlo Calculations for Alcohols and Their Mixtures with Alkanes. Transferable Potentials for Phase Equilibria. 5. United-Atom Description of Primary, Secondary, and Tertiary Alcohols. *J Phys Chem B*. **2001**, *105*, 3093 - 3104.
- Crowell, A. D. Potential Energy Functions for Graphite. *J Chem Phys* **1958**, *29*, 446-447.
- Deitz, V. R. The Adsorption of Carbon Dioxide on Carbon Solids. I. Graphite and Diamond at 0.Degree. *J Phys Chem*. **1967**, *71*, 830-837.
- Dell, R. M.; Beebe, R. A. Heats of Adsorption of Polar Molecules on Carbon Surfaces .2. Ammonia and Methylamine. *J Phys Chem-US*. **1955**, *59*, 754-762.
- Do, D. D. *Adsorption Analysis : Equilibria and Kinetics*; Singapore : World Scientific 1998
- Do, D. D.; Do, H. D. Modeling of Adsorption on Nongraphitized Carbon Surface: GCMC Simulation Studies and Comparison with Experimental Data. *J Phys Chem B*. **2006**, *110*, 17531-17538.
- Do, D. D.; Do, H. D. Effects of Potential Models on the Adsorption of Carbon Dioxide on Graphitized Thermal Carbon Black: GCMC Computer Simulations. *Colloids Surfaces A*. **2006**, *277*, 239-248.
- Do, D. D.; Nicholson, D.; Do, H. D. On the Henry Constant and Isothermic Heat at Zero Loading in Gas Phase Adsorption. *J Colloid Interf Sci*. **2008**, *324*, 15-24.
- Donnet, J. B. Fifty Years of Research and Progress on Carbon Black. *Carbon*. **1994**, *32*, 1305-1310.
- Donnet, J. B. *Carbon Black: Science and Technology*; CRC Press 1993
- Easton, E. B.; Machin, W. D. Adsorption of Water Vapor on a Graphitized Carbon Black. *J Colloid Interf Sci*. **2000**, *231*, 204-206.
- Emmett, P. H.; Anderson, R. B. The Adsorption of Water Vapor on Carbon Black. *J Am Chem Soc*. **1945**, *67*, 1492-1494.
- Emmett, P. H. Adsorption and Pore Size Measurements on Charcoals and Whetlerites. *Chem Rev*. **1948**, *43*, 69-148.
- Everett, D. H.; Powl, J. C. Adsorption in Slit-Like and Cylindrical Micropores in the Henry's Law Region. A Model for the Microporosity of Carbons. *J Chem Soc Farad T 1*. **1976**, *72*, 619-636.
- Fan, C.; Razak, M. A.; Do, D. D.; Nicholson, D. On the Identification of the Sharp Spike in the Heat Curve for Argon, Nitrogen, and Methane Adsorption on Graphite: Reconciliation between Computer Simulation and Experiments. *J Phys Chem B*. **2011**, *116*, 953-962.
- Gardner, L.; Kruk, M.; Jaroniec, M. Reference Data for Argon Adsorption on Graphitized and Nongraphitized Carbon Blacks. . *J Phys Chem B*. **2001**, *105*, 12516-12523.
- Gale, R.; Beebe, R. Determination of heats of adsorption on carbon blacks and bone mineral by chromatography using the eluted pulse technique. *J. Phys. Chem*. **1964**, *68*, 555-67.
- Graham, D.; Kay, W. The morphology of thermally graphitized P-33 carbon black in relation to its adsorbent uniformity. *J. Coll. Sci*. **1961**, *16*, 182-5.
- Grillet, Y.; Rouquerol, F.; Rouquerol, J. Two-Dimensional Freezing of Nitrogen or Argon on Differently Graphitized Carbons. *J Colloid Interf Sci*. **1978**, *70*, 239-244.
- Gumma, S.; Talu, O. Net Adsorption: A Thermodynamic Framework for Supercritical Gas Adsorption and Storage in Porous Solids. *Langmuir*. **2010**, *26*, 17013-17023.
- Healey, F. H.; Yu, Y.-F.; Chessick, J. J. The Detection of Hydrophilic Heterogeneities on a Carbon Surface. *J Phys Chem-US*. **1955**, *59*, 399-402.

- Holmes, J. M.; Beebe, R. A. An Example of Desorption Hysteresis at Low Relative Pressure on a Non-Porous Adsorbent - Ammonia on Graphitized Carbon Black. *J Phys Chem-US*. **1957**, *61*, 1684-1686.
- Horikawa, T; Zeng, Y.; Do, D. D.; Sotowa, K.; Avila, J. On the isosteric heat of adsorption of non-polar and polar fluids on highly graphitized carbon black. *J Coll. Interface Sci*. **2015**, *439*, 1-6.
- Isirikyan, A. A.; Kiselev, A. V. Adsorption Isotherms of Nitrogen, Benzene and N-Hexane and the Heats of Adsorption of Benzene and N-Hexane on Graphitized Carbon Blacks. Ii. Adsorption on Graphitized Channel Blacks. *J Phys Chem-US*. **1962**, *66*, 205-209.
- Jorge, M.; Schumacher, C.; Seaton, N. A. Simulation Study of the Effect of the Chemical Heterogeneity of Activated Carbon on Water Adsorption. *Langmuir*. **2002**, *18*, 9296-9306.
- Jorgensen, W. L.; Madura, J. D.; Swenson, C. J. Optimized Intermolecular Potential Functions for Liquid Hydrocarbons. *J Am Chem Soc*. **1984**, *106*, 6638-6646.
- Jorgensen, W. L. Optimized Intermolecular Potential Functions for Liquid Alcohols. *J Phys Chem-US*. **1986**, *90*, 1276-1284.
- Juhola, A. J.; Wiig, E. O. Pore Structure in Activated Charcoal. I. Determination of Micro Pore Size Distribution. *J Am Chem Soc*. **1949**, *71*, 2069-2077.
- Kristof, T.; Vorholz, J.; Liszi, J.; Rumpf, B.; Maurer, G. A Simple Effective Pair Potential for the Molecular Simulation of the Thermodynamic Properties of Ammonia. *Mol Phys*. **1999**, *97*, 1129-1137.
- Kruchten, F.; Knorr, K. Multilayer Adsorption and Wetting of Acetone on Graphite. *Phys Rev Lett*. **2003**, *91*, 085502-1-085502-4.
- Kruk, M.; Li, Z.; Jaroniec, M. Nitrogen Adsorption Study of Surface Properties of Graphitized Carbon Blacks. *Langmuir*. **1999**, *15*, 1435-1441.
- Langmuir, I. The Constitution and Fundamental Properties of Solids and Liquids. Ii. Liquids.1. *J Am Chem Soc*. **1917**, *39*, 1848-1906.
- Larher, Y. Phase Transitions" between Dense Monolayers of Atoms and Simple Molecules on the Cleavage Face of Graphite, with Particular Emphasis on the Transition of Nitrogen from a Fluid to a Registered Monolayer. *J Chem Phys*. **1978**, *68*, 2257-2263.
- Larsen, M. J.; Skou, E. M. ESR, XPS, and Thin-Film Characterization of Nano Structured Carbon Materials for Catalyst Support in PEM Fuel Cells. *J Power Sources*. **2012**, *202*, 35-46.
- Liu, J. C.; Monson, P. A. Monte Carlo Simulation Study of Water Adsorption in Activated Carbon. *Ind Eng Chem Res*. **2006**, *45*, 5649-5656.
- Lodewyckx, P.; Vansant, E. F. Water Isotherms of Activated Carbons with Small Amounts of Surface Oxygen. *Carbon*. **1999**, *37*, 1647-1649.
- Lopez-Gonzalez, J.; Carpenter, F.; Dietz, V. Adsorption of nitrogen and argon on mineralogical graphite and diamond at 77 and 90K. *J. Phys. Chem*. **1961**, *65*, 1112-9.
- Malbrunot, P.; Vidal, D.; Vermesse, J.; Chahine, R.; Bose, T. K. Adsorption Measurements of Argon, Neon, Krypton, Nitrogen, and Methane on Activated Carbon up to 650 Mpa. *Langmuir*. **1992**, *577*-580.
- Malbrunot, P.; Vidal, D.; Vermesse, J.; Chahine, R.; Bose, T. K. Adsorbent Helium Density Measurement and Its Effect on Adsorption Isotherms at High Pressure. *Langmuir*. **1997**, *13*, 539-544.

- McCallum, C. L.; Bandosz, T. J.; McGrother, S. C.; Müller, E. A.; Gubbins, K. E. A Molecular Model for Adsorption of Water on Activated Carbon: Comparison of Simulation and Experiment. *Langmuir*. **1998**, *15*, 533-544.
- Meyer, E.; Deitz, V. Anisotropy in physical adsorption on graphite. *J. Phys. Chem.* **1967**, *71*, 1521-3.
- Millard, B.; Beebe, R. A.; Cynarski, J. The Heat of Adsorption of Methanol on Carbon Adsorbents at 0°. *J Phys Chem.* **1954**, *58*, 468-471.
- Millard, B.; Caswell, E. G.; Leger, E. E.; Mills, D. R. The Adsorption and Heats of Adsorption of Water on Spheron 6 and Graphon. *J Phys Chem-US.* **1955**, *59*, 976-978.
- Miura, K.; Morimoto, T. Adsorption Sites for Water on Graphite. 3. Effect of Oxidation Treatment of Sample. *Langmuir*. **1986**, *2*, 824-828.
- Miura, K.; Morimoto, T. Adsorption Sites for Water on Graphite .4. Chemisorption of Water on Graphite at Room Temperature. *Langmuir*. **1988**, *4*, 1283-1288.
- Miura, K.; Morimoto, T. Adsorption Sites for Water on Graphite. 5. Effect of Hydrogen-Treatment of Graphite. *Langmuir*. **1991**, *7*, 374-379.
- Morimoto, T.; Miura, K. Adsorption Sites for Water on Graphite. 1. Effect of High-Temperature Treatment of Sample. *Langmuir*. **1985**, *1*, 658-662.
- Morimoto, T.; Miura, K. Adsorption Sites for Water on Graphite .2. Effect of Autoclave Treatment of Sample. *Langmuir*. **1986**, *2*, 43-46.
- Mooney, D. A.; Müller-Plathe, F.; Kremer, K. Simulation Studies for Liquid Phenol: Properties Evaluated and Tested over a Range of Temperatures. *Chem Phys Lett.* **1998**, *294*, 135-142.
- Muller, E. A.; Rull, L. F.; Vega, L. F.; Gubbins, K. E. Adsorption of water on activated carbons: A molecular simulation study. *J. Phys. Chem.* **1996**, *100*, 1189-1196.
- Myers, A.; Prausnitz, J. Hindered rotation in physical adsorption. *Trans. Farad. Soc.* **1965**, *61*, 755-64.
- Nakada, K.; Fujita, M.; Dresselhaus, G.; Mildred, D. S. Edge State in Graphene Ribbons: Nanometer Size Effect and Edge Shape Dependence. *Phys Rev B.* **1996**, *54*, 17954-17961.
- Naono, H.; Shimoda, M.; Morita, N.; Hakuman, M.; Nakai, K.;Kondo, S. Interaction of Water Molecules with Nongraphitized and Graphitized Carbon Black Surfaces†. *Langmuir*. **1997**, *13*, 1297-1302.
- Nguyen, T. X.; Bhatia, S. K. How Water Adsorbs in Hydrophobic Nanospaces. *Journal of Physical Chemistry C* **2011**, *115* (33), 16606-16612.
- Nguyen, V. T.; Do, D. D.; Nicholson, D. On the Heat of Adsorption at Layering Transitions in Adsorption of Noble Gases and Nitrogen on Graphite. *J Phys Chem B.* **2010**, *114*, 22171-22180.
- Nguyen, V. T.; Do, D. D.; Nicholson, D.; Jagiello, J. Effects of Temperature on Adsorption of Methanol on Graphitized Thermal Carbon Black: A Computer Simulation and Experimental Study. *J Phys Chem B.* **2011**, *115*, 16142-16149.
- Nguyen, V. T.; Do, D. D.; Nicholson, D. A New Molecular Model for Water Adsorption on Graphitized Carbon Black. *Carbon.* **2014**, *66*, 629-636.
- Nguyen, V. T.; Horikawa, T.; Do, D. D.; Nicholson, D. Water as a Potential Molecular Probe for Functional Groups on Carbon Surfaces. *Carbon.* **2014**, *67*, 72-78.
- Nguyen, V. T.; Horikawa, T.; Do, D. D.; Nicholson, D. On the Relative Strength of Adsorption of Gases on Carbon Surfaces with Functional Groups: Fluid–Fluid, Fluid–Graphite and Fluid–Functional Group Interactions. *Carbon.* **2013**, *61*, 551-557.

- Ohba, T.; Kaneko, K. Surface Oxygen-Dependent Water Cluster Growth in Carbon Nanospaces with GCMC Simulation-Aided in Situ SAXS. *J Phys Chem B*. **2007**, *111*, 6207-6214.
- Ohba, T.; Kanoh, H. Intensive Edge Effects of Nanographenes in Molecular Adsorptions. *J Phys Chem Lett*. **2012**, *3*, 511-516.
- Pace, E. L.; Siebert, A. R. Heats of Adsorption and Adsorption Isotherms for Low Boiling Gases Adsorbed on Graphon. *J Phys Chem-US*. **1960**, *64*, 961-963.
- Pierce, C.; Wiley, J. W.; Smith, R. N. Capillarity and Surface Area of Charcoal. *J Phys Colloid Chem*. **1949**, *53*, 669-683.
- Pierce, C.; Smith, R. N. Heats of Adsorption .iii. Methanol on Carbon. *J Phys Colloid Chem*. **1950**, *54*, 354-364.
- Pierce, C.; Smith, R. N. Adsorption-Desorption Hysteresis in Relation to Capillarity of Adsorbents. *J Phys Colloid Chem*. **1950**, *54*, 784-794.
- Pierce, C.; Smith, R. N.; Wiley, J. W.; Cordes, H. Adsorption of Water by Carbon1. *J Am Chem Soc*. **1951**, *73*, 4551-4557.
- Polley, M. H.; Schaeffer, W. D.; Smith, W. R. Development of Stepwise Isotherms on Carbon Black Surfaces. *J Phys Chem-US*. **1953**, *57*, 469-471.
- Potoff, J. J.; Siepmann, J. I. Vapor - Liquid Equilibria of Mixtures Containing Alkanes, Carbon Dioxide and Nitrogen. *AIChE*. **2001**, *47*, 1676-1683.
- Ross, S.; Winkler, W. On Physical Adsorption : Viii. Monolayer Adsorption of Argon and Nitrogen on Graphitized Carbon. *J Colloid Sci*. **1955**, *10*, 319-329.
- Ross, S.; Pultz, W. W. On Physical Adsorption : X. Adsorbed Monolayers of Argon and Nitrogen on Boron Nitride and on a Graded Series of Partially Graphitized Carbon Blacks. *J Colloid Sci*. **1958**, *13*, 397-406.
- Rouquerol, J.; Partyka, S.; Rouquerol, F. Calorimetric Evidence for a Bidimensional Phase-Change in Monolayer of Nitrogen or Argon Adsorbed on Graphite at 77k. *J Chem Soc Farad T 1*. **1977**, *73*, 306-314.
- Rouquerol, J.; Rouquerol, F.; Sing, K. *Adsorption by Powders & Porous Solids*. Academic Press, New York, 2013.
- Salame, I. I.; Bagreev, A.; Bandosz, T. J. Revisiting the Effect of Surface Chemistry on Adsorption of Water on Activated Carbons. *J Phys Chem B*. **1999**, *103*, 3877-3884.
- Salame, I. I.; Bandosz, T. J. Interactions of Water, Methanol and Diethyl Ether Molecules with the Surface of Oxidized Activated Carbon. *Mol Phys*. **2002**, *100*, 2041-2048.
- Sarakhov, A. I.; Dubinin, M. M.; Berezkina, Y. F.; Zaverina, E. D. Adsorption of Vapors on Nonporous Sorbent Models with a Physically Modified Surface. *B Acad Sci USSR CH+*. **1961**, *10*, 902-910.
- Sarakhov, A. I.; Dubinin, M. M.; Berezkina, Y. F. Vapor Adsorption of Nonporous Adsorbent Models with Physically Modified Surfaces. Communication 2. Low Temperature Adsorption of Nitrogen on Carbon Black with Preadsorbed Benzene and Methyl Alcohol. *B Acad Sci USSR CH+*. **1963**, *12*, 1069-1076.
- Schaeffer, W. D.; Smith, W. R.; Polley, M. H. Structure and Properties of Carbon Black - Changes Induced by Heat Treatment. *Ind Eng Chem*. **1953**, *45*, 1721-1725.
- Segarra, E. I.; Glandt, E. D. Model Microporous Carbons: Microstructure, Surface Polarity and Gas Adsorption. *Chem Eng Sci*. **1994**, *49*, 2953-2965.

- Seredych, M.; Jagiello, J.; Bandosz, T. J. Complexity of CO<sub>2</sub> Adsorption on Nanoporous Sulfur-Doped Carbons – Is Surface Chemistry an Important Factor? *Carbon*. **2014**, *74*, 207-217.
- Sing, K. Physisorption of gases by carbon blacks. *Carbon*, **1994**, *32*, 1311-7.
- Smith, R. N.; Pierce, C. Heats of Adsorption. II. *J Phys Colloid Chem*. **1948**, *52*, 1115-1128.
- Smith, R. N.; Duffield, J.; Pierotti, R. A.; Mool, J. Carbon–Oxygen and Carbon–Hydrogen Surface Complexes. *J Phys Chem-US*. **1956**, *60*, 495-497.
- Spencer, W. B.; Amberg, C. H.; Beebe, R. A. Further Studies of Adsorption on Graphitized Carbon Blacks. *J Phys Chem-US*. **1958**, *62*, 719-723.
- Steele, W. A.; Halsey, G. D. The Interaction of Gas Molecules with Capillary and Crystal Lattice Surfaces. *J Phys Chem-US*. **1955**, *59*, 57-65.
- Taqvi, S. M.; LeVan, M. D. Virial Description of Two-Component Adsorption on Homogeneous and Heterogeneous Surfaces. *Ind Eng Chem Res*. **1997**, *36*, 2197-2206.
- Tóth, A.; László, K. Chapter 5 - Water Adsorption by Carbons. Hydrophobicity and Hydrophilicity. In *Novel Carbon Adsorbents*. Edited by Tascón JMD. Oxford: Elsevier; **2012**, 147-171.
- Ustinov, E.; Do, D. D. Simulation of gas adsorption on a surface and in slit pores with grand canonical and canonical kinetic Monte Carlo methods. *Phys. Chem. Chem. Phys.* **2012**.
- Volkman, U. G.; Knorr, K. Wetting Transition of C<sub>2</sub>Cl<sub>2</sub> on Graphite. *Phys Rev B*. **1993**, *47*, 4011-4013.
- Yoshizawa, N.; Tanaike, O.; Hatori, H.; Yoshikawa, K.; Knodo, A.; Abe, T. TEM observation of heterogeneous polyhedronization behaviour in graphitized carbon nanospheres. *Mat. Sci. Eng. B*, **2008**, *148*, 245-8.
- Yoshizawa, N.; Soneda, Y.; Hatori, H.; Ue, H.; Abe, T. Development and degradation of graphitic microtexture in carbon nanospheres under a morphologically restrained condition. *Mat. Chem. Phys.* **2010**, *121*, 419-24.
- Yoshizawa, N.; Hatori, H.; Yoshikawa, K.; Miura, K.; Abe, T. TEM and electron tomography studies of carbon nanospheres for lithium secondary batteries. *Carbon*. **2006**, *44*, 2558-64.
- Young, G. J.; Chessick, J. J.; Healey, F. H.; Zettlemoyer, A. C. Thermodynamics of the Adsorption of Water on Graphon from Heats of Immersion and Adsorption Data. *J Phys Chem*. **1954**, *58*, 313-315.
- Zeng, H.; Prasetyo, L.; Nguyen, V.; Horikawa, T.; Do, D. D.; Nicholson, D. Characterization of oxygen functional groups on carbon surfaces with water and methanol adsorption. *Carbon*. **2015**, *81*, 447-57.
- Zettlemoyer, A. C. Hydrophobic Surfaces. *J Colloid Interf Sci*. **1968**, *28*, 343-369.
- Zhao, X. Wetting Transition of Water on Graphite: Monte Carlo Simulations. *Phys Rev B*. **2007**, *76*, 041402-1-041402-4.



## Appendix 1

The molecular parameters for carbon dioxide, methanol, ammonia and water are given in the following table.

Parameter	Units	
<b>N<sub>2</sub></b>		
$\sigma$ of N	nm	0.331
$\epsilon/k_B$ of N	K	36
q of N	e	-0.482
q of COM of N <sub>2</sub>	e	0.964
R <sub>N-N</sub>	nm	0.11
<b>CO<sub>2</sub></b>		
$\sigma$ of C	nm	0.28
$\epsilon/k_B$ of C	K	27
$\sigma$ of O	nm	0.305
$\epsilon/k_B$ of O	K	79
q of C	e	0.7
q of O	e	-0.35
R <sub>C-O</sub>	nm	0.116
<b>Methanol</b>		
$\sigma$ of CH <sub>3</sub>	nm	0.375
$\epsilon/k_B$ of CH <sub>3</sub>	K	98
$\sigma$ of O	nm	0.302
$\epsilon/k_B$ of O	K	93
q of CH <sub>3</sub>	e	0.265
q of O	e	-0.70
q of H	e	0.435
R <sub>C-O</sub>	nm	0.143
R <sub>O-H</sub>	nm	0.0945
$\angle$ COH	degree	108.5
<b>Ammonia</b>		
$\sigma$ of N	nm	0.3385
$\epsilon/k_B$ of N	K	170
q of N	e	-1.035
q of H	e	0.345
R <sub>N-H</sub>	nm	0.10124
$\angle$ HNH	degree	106.68
<b>Water</b>		
$\sigma$ of O	nm	0.3166
$\epsilon/k_B$ of O	K	78.23
q of O	e	-0.8476
q of H	e	0.4238
R <sub>O-H</sub>	nm	0.1
$\angle$ HOH	degree	109.47

Methanol from Chen *et al.* (2001); water from Berendsen *et al.* (1987) 6269; ammonia from Kristoff *et al.* (1999); CO<sub>2</sub> from Potoff *et al.* (2001).

Graphical abstract

